学位論文

Mechanism of pavement cell morphogenesis and stomatal distribution patterning in plant leaf epidermis

葉の表皮組織における細胞形態と気孔分布に関する研究

平成 25 年 12 月　博士（生命科学）申請

東京大学大学院新領域創成科学研究科
先端生命科学専攻

秋田　佳恵

Mechanism of pavement cell morphogenesis and stomatal distribution patterning in plant leaf epidermis

Kae Akita

2013

Department of Integrated Biosciences,

Graduate School of Frontier Sciences,

The University of Tokyo

Acknowledgements

I first wish to express my deepest appreciation to Prof. Seiichiro Hasezawa (The University of Tokyo) for his guidance and encouragement throughout this study.

I thank to Dr. Natsumaro Kustuna (The University of Tokyo) for his instruction and support, and Dr. Takumi Higaki (The University of Tokyo) for his critical advice and useful discussion.

I am grateful to Dr. Takashi Ueda and Dr. Kazuo Ebine (The University of Tokyo), for providing seeds of transgenic *Arabidopsis* expressing ST-mRFP or ERD2-GFP. I thank to Prof. Ikuko Hara-Nishimura (Kyoto University), for providing seeds of transgenic *Arabidopsis* expressing ST-GFP. I thank to Prof. Takashi Hashimoto (Nara Institute of Science and Technology), for providing seeds of transgenic *Arabidopsis* expressing GFP-tubulinβ. I am grateful to Dr. Noriko Nagata, Dr. Mamiko Sato, and Ms. Megumi Kobayashi (Japan Women's University), and Dr. Kiminori Toyooka, Dr. Mayuko Sato, and Ms. Mayumi Wakazaki (RIKEN) for experimental support of transmission electron microscopy.

I also appreciate all of the members of the Laboratory of Plant Cell Biology in Totipotency for their help and encouragement.

Finally, I want to thank my family and friends for their continuous support through this study.

Contents

Abbreviations

ABP1, AUXIN BINDING PROTEIN 1

BASL, BREAKING OF ASYMMETRY IN THE STOMATAL LINEAGE

BY-2, Bright Yellow 2

CCD, charge coupled device

CHOR, CHORUS

CLSM, confocal laser scanning microscopy

DAG, day after germination

DMSO, dimethyl sulfoxide

ER, endoplasmic reticulum

ERD2, ENDOPLASMIC RETICULUM RETENTION DEFECTIVE 2

EPF, EPIDERMAL PATTERNING FACTOR

FDA, fluorescein diacetate

FM4-64,

N-(3-triethylammoniumpropyl)-4-(6-(4-(diethylamino)phenyl)hexatrienyl)-pyridinium dibromide

GFP, green fluorescent protein

GSL8, GLUCAN SYNTHASE-LIKE 8

IgG, immunoglobulin G

MAP, mitogen-activated protein

MAPK, mitogen-activated protein kinase

MAPKK, mitogen-activated protein kinase kinase

MAPKKK, mitogen-activated protein kinase kinase kinase

MVB, multi vesicular body

mRFP, monomeric red fluorescent protein

PI3K, phosphatidylinositol 3-kinase

PI4K, phosphatidylinositol 4-kinase

PIN1, PINFORMED 1

PIP2a, plasma membrane intrinsic protein 2a

PMB, paramural body

RIC, ROP-interactive CRIB motif-containing proteins

ROP, Rho-related GTPase from plants

SCRM, SCREAM

SPCH, SPEECHLESS

ST, rat sialyltransferase

SuSy, sucrose synthase

TEM, transmission electron microscopy

TMM, TOO MANY MOUTHS

UDP, uridine diphosphate

General introduction

Leaves are the most important photosynthetic organs in the majority of flowering plants. To receive more sunlight, plants must expand their leaf area. In this process, the leaf epidermis extends in a single layer and covers the mesophyll cells that are specialized for photosynthesis. Leaf epidermis mainly consists of pavement cells and guard cells. Pavement cells are flat but, in most dicot plants, interdigitated with adjacent pavement cells like a jigsaw puzzle. They have multi-polarity and several local expansion sites, indicating a unique growth pattern. Paired guard cells surround stomata and change their shape to regulate stomatal opening and closing to control the gas exchange, which affects photosynthesis. This study was intended to elucidate the cellular mechanisms of pavement cell morphogenesis and of stomatal distribution patterning in the epidermis during leaf expansion.

Plant cells grow either by diffuse growth or tip growth. Diffuse growth is observed in various plant cell types; its direction is determined by the orientation of cellulose microfibrils in the cell wall that align parallel to microtubules in the cell cortex. In contrast, tip growth occurs mainly in root hairs and pollen tubes. In this pattern of polarized cell expansion, the apical region is filled with secretory vesicles that provide new plasma membrane and secrete new wall materials. Previous molecular cell biological studies have indicated that jigsaw puzzle-shaped leaf pavement cell morphogenesis requires both cytoskeleton orientation and membrane trafficking (Fu et al. 2005, 2009, Xu et al. 2010). However, the existence of a local secretory pathway in pavement cells, as in tip growth cells, was still unclear, and quantitative measurements of microtubule orientation in pavement cells

were not sufficient. Therefore in this study, I performed visualization and quantitative analyses of exocytosis and microtubules in pavement cells.

In addition, I studied on stomatal distributional patterning. In most dicot plants, stomata follow the "one-cell-spacing rule" in which they are separated by at least one intervening non-stomatal lineage cell, such as pavement cells (Sachs, 1991). This distribution is affected by genes that regulate stomatal differentiation and patterning (Lau and Bergmann, 2012, Torii, 2012). In this study, I found that abnormal clustered stomata were observed in *Arabidopsis* leaves that were immersed in sucrose solution at the stage of cell differentiation into guard cells or pavement cells. Based on my observations, I will discuss how external conditions affect the stomatal distribution patterning.

References

Fu Y, Gu Y, Zheng Z, Wasteneys G, Yang Z (2005) *Arabidopsis* interdigitating cell growth requires two antagonistic pathways with opposing action on cell morphogenesis. *Cell* 120:687–700

Fu Y, Xu T, Zhu L, Wen M, Yang Z (2009) A ROP GTPase signaling pathway controls cortical microtubule ordering and cell expansion in *Arabidopsis*. *Curr Biol* 19:1827–1832

Lau OS, Bergmann DC (2012) Stomatal development: a plant's perspective on cell polarity, cell fate transitions and intercellular communication. *Development* 139:3683–3692

Sachs T (1991) Pattern formation in plant tissues. *Cambridge University*

Press, Cambridge, UK.

Torii KU (2012) Mix-and-match: ligand-receptor pairs in stomatal development and beyond. *Trends Plant Sci* 17:711–719

Xu T, Wen M, Nagawa S, Fu Y, Chen JG, Wu MJ, Perrot-Rechenmann C, Friml J, Jones AM, Yang Z (2010) Cell surface- and rho GTPase-based auxin signaling controls cellular interdigitation in *Arabidopsis*. *Cell* 143:99–110

Chapter I: Accumulations of Golgi body-localized fluorescent proteins in interdigitated apoplastic region in *Arabidopsis* leaf epidermis

Abstract

Leaf epidermal pavement cells have jigsaw puzzle-like shapes in dicotyledonous plants. However, the cell biological processes underlying their morphogenesis are largely unknown. I found the apoplastic localization of monomeric red fluorescent protein (mRFP)-tagged rat sialyl transferases (ST-mRFP), which are a marker of the *trans*-Golgi membrane. The apoplastic localization became pronounced at both ends of the guard cells and at the curved pavement cell border during cell maturation. I performed immunoelectron microscopic analysis on the *Arabidopsis* leaf epidermis with mRFP-antibodies. The gold particle signals were mainly detected in the apoplast of young leaves, whereas they were detected both in apoplast and cell walls in mature leaves. These results suggested that the secretory pathway to the apoplastic region is involved in pavement cell morphogenesis. To gain insight into the ultra-micro structures involved in pavement cell morphogenesis, I performed transmission electron microscopy (TEM) observations of *Arabidopsis* leaf epidermis. TEM observations revealed the existence of many vesicular membrane structures called paramural bodies (PMBs) between the plasma membrane and cell wall. PMBs were more frequently observed in young leaves than in mature leaves.

Introduction

Plant cell growth requires the secretion of the new plasma membrane and materials of cell wall into the extracellular space. In this process, called exocytosis, secretory vesicles move to the plasma membrane and release their contents extracellularly by membrane fusion. Exocytosis has been commonly observed in apical regions of tip growing cells in root hairs and pollen tubes, where Golgi bodies and secretory vesicles derived from them are found (Lancelle and Hepler, 1992, Parton et al. 2001, 2003). In another study of exocytosis, secretory vesicle clusters in tobacco BY-2 cells contained protein and polysaccharides (Toyooka et al. 2009). In the space outside the plasma membrane called apoplast regions, RFP tagged with secretory signal was observed in *Arabidopsis* (Samalova et al. 2006).

Multivesicular bodies (MVBs) are spherical endosomal organelles containing several small vesicles in plant and animal cells. In animal cells, MVBs function into exocytosis and endocytosis, by which extracellular material is internalized. When MVBs fuse to the plasma membrane during exocytosis, the released vesicles are called exosomes (Marchant et al. 1967, Harding et al. 1983). In plant cells, although MVBs play a role endocytosis (Tanchak et al. 1984), their involvement in exocytosis was unclear. In contrast, PMBs are structures in which several small vesicles are situated in the paramural space between the cell wall and plasma membrane. MVBs and PMBs were observed during cell plate formation in cell division (Samuels et al. 1995), and during secondary wall thickening (Robards et al. 1969). In addition, PMBs also appeared during plant defense against powdery mildew infection (An et al. 2006a, 2006b). These studies suggested

that MVBs work as exosomes and fuse with the plasma membrane to result in the appearance of PMBs in plant cells.

In this study, I used live imaging with confocal laser scanning microscopy (CLSM) and observation of ultra-micro structures with TEM to examine exocytosis associated with pavement cell morphogenesis.

Materials and Methods

Plant materials and growth conditions

Seeds of transgenic *Arabidopsis thaliana* plants expressing ST-mRFP or ENDOPLASMIC RETICULUM RETENTION DEFECTIVE 2 (ERD2)-green fluorescent protein (ERD2-GFP) were kindly provided by Dr. Takashi Ueda (The University of Tokyo). Seeds of transgenic *Arabidopsis thaliana* plants expressing ST-GFP were kindly provided by Prof. Ikuko Hara-Nishimura (Kyoto University). Wild type (Col-0) or transgenic *Arabidopsis* plants were grown on soil/vermiculite as described by Naito et al. (1994) in growth chambers at 23.5°C with 60% relative humidity and a 12 h light/12 h dark cycle, using 100 μmol m^{-2} s^{-1} white lights.

Fluorescence microscopy and image analysis

To acquire confocal images, I used a fluorescence microscope (IX70, Olympus, Tokyo, Japan) equipped with an UplanApo 40× iris objective lens and a CSU10 scanning head (Yokogawa, Tokyo, Japan) together with a cooled CCD camera head system (CoolSNAP HQ, PhotoMetrics, Tucson, U.S.A.). The data were processed using ImageJ software (Abramoff et al. 2004) with JAVA plug-ins (http://hasezawa.ib.k.u-tokyo.ac.jp/zp/Kbi).

Cell staining

To visualize plasma membrane, cells were stained with 32 μM FM4-64 dye (Life Technologies, Tokyo, Japan) in basal buffer [5mM MES-Tris, 10 mM $CaCl_2$, 50 mM KCl, pH6.5] at room temperature for 5–10 min. To visualize apoplast, leaf epidermis of wild type (Col-0) were stained with 1 g/L Alexa-488-dextran in basal buffer at room temperature for 4 h.

Plasmolysis and fluorescein diacetate (FDA) staining

Leaves expressing ST-mRFP were mounted in 0.85 M sodium chloride solution supplemented with 10 μg/mL FDA dye for 10 min to achieve plasmolysis and cytoplasm visualization.

Preparation and fluorescent measurement of apoplast fluid

Apoplast fluid was collected from the leaves according to a procedure similar to that described by Nishitani and Tominaga (1991). Briefly, 0.5 g of mature leaves from 45-day-old *Arabidopsis* plants were excised with a razor. The excised leaves were put in a 67 μm nylon mesh bag and washed three times with 10 mM potassium phosphate buffer (pH 6.0). The leaves were packed into a 10 mL plastic syringe tube and infiltrated under reduced pressure for 5 min. Then, 50 mM $MgCl_2$ (100 μl) was poured onto the packed leaves in the tube. They were then centrifuged at 800 ×*g* for 10 min at 4°C. A total of 150–200 μL of apoplastic solution was collected. Aliquots of 66 μl of apoplastic solution were transferred to a 96-well imaging plate (Sumilon Multi Well Plate, Sumitomo Bakelite, Tokyo, Japan). Fluorescence images of

the wells were captured with a fluorescent microscope (IX-70, Olympus) equipped with a color CCD camera (DP-70, Olympus). The fluorescent intensity was measured with ImageJ software.

Transmission electron microscopy

Leaves were cut out into 0.5 mm squares, and then prefixed with 4% paraformaldehyde and 2% glutaraldehyde at 4°C overnight. The samples were postfixed with 2% osmium tetroxide at 4°C overnight. The samples were dehydrated through an ethanol series and embedded in Spurr resin, and the resin was polymerized at 72°C for 12 h. Thin sections (0.5 μm thick) were cut with a diamond knife, stained with 4% uranyl acetate for 18 min and a lead citrate solution for 7 min. For immunoelectron microscopy, fixed samples were embedded in LR White resin, the resin was polymerized at 50°C for 24 h, and incubated with rat mRFP antibody (5F8; ChromoTek, Martinsried, Germany) at room temperature for 30 min. After that, the sample were incubated with goat immunoglobulin G (IgG) to bond gold particles at room temperature for 1 h. Thin sections stained with 4% uranyl acetate for 5–10 min. These samples were observed with an electron microscope (JEM-1200 EX; JEOL Ltd., Tokyo, Japan).

For high-pressure freezing, the leaves were immersed in sugar solution at room temperature for 1–2 h. These leaves were cut out into 0.5 mm squares. The samples were frozen in a high-pressure freezer (EM-PACT; Leica, Tokyo, Japan). The frozen samples were substituted with 2% osmium tetroxide in acetone at -80ºC for 2-4 days, stained with 1% tannic acid in acetone at room temperature for 1 h, and then embedded in epoxy resin at 60 ºC for 24 h. Thin sections were stained with 1% uranyl acetate.

Inhibitor treatments

Using a 96-well plate (Sumilon Multi Well Plate, Sumitomo Bakelite, Tokyo, Japan), *Arabidopsis* seeds were germinated in distilled water containing inhibitors. The seedling were treated with 30 μM wortmannin (Wako Pure Chemical Ind., Osaka, Japan) for 7 days, and then observed.

Results

ST-mRFP localized in Golgi bodies and apoplastic regions

To visualize the exocytosis pathway in pavement cells, I observed *Arabidopsis* expressing the *trans*-Golgi marker ST-mRFP by CLSM. ST-mRFP fluorescence highlighted leaf pavement cell borders and both ends of the guard cells (Fig. I-1A), in addition to, *trans*-Golgi bodies as previously reported (Boevink et al. 1998, Latijnhouwers et al. 2005). In *Arabidopsis* expressing ST-GFP or the *cis*-Golgi marker ERD2-GFP, dot-like Golgi bodies were fluorescently labeled but the cell borders were not (Fig. I-S1). After plasmolysis, mRFP fluorescence was observed in the apoplastic space between cell walls and plasmolyzed cells stained with FDA (Fig. I-1B). Fluorescence of mRFP was notable in the extracted apoplast fluid from ST-mRFP expression lines but not from wild type (Col-0) (Fig. I-1C), suggesting that the red fluorescence was not autofluorescence. The localizations were confirmed by immuno-electron microscopy. Ultrathin sections of leaves of ST-mRFP expression lines were chemically fixed and stained with an anti-mRFP immunogold antibody. The gold particles labeled cell walls sandwiched between pavement cells (Fig. I-1D). Furthermore, the

ends of guard cells were also labeled with the gold particles (Fig. I-1E). These results showed that ST-mRFP proteins moved to extracellular region via *trans*-Golgi bodies.

Localization of ST-mRFP changed with epidermal cell maturation

Rosette leaves of a 45-day-old *Arabidopsis* plant were classified based on leaf length as "young leaf" (2–3 mm in length; Fig. I-2A), "mid-sized leaf" (8–10 mm; Fig. I-2C), and "mature leaf" (27–30 mm; Fig. I-2E). The apoplastic localizations of ST-mRFP became more prominent during leaf growth (Fig. I-2B, D, F). These results suggested that extracellular ST-mRFP proteins gradually accumulate during epidermal cell maturation.

mRFP fluorescent intensity increased with cell border curvature

In mature leaves, mRFP fluorescence seemed to accumulate in curved apoplastic regions (Fig. I-1A). To visualize the size of apoplastic regions, I observed plasma membrane labeled with plasma membrane intrinsic protein 2a (PIP2a) tagged by GFP (GFP-PIP2a), and apoplast stained with 1 g/L Alexa488-dextran for 4 h (Fig. I-S2). There was little difference in width between the curved and non-curved regions at the same magnification used in CLSM. To investigate the relationship between mRFP fluorescence and cell border geometry, the mRFP fluorescent intensity and cell border curvature were simultaneously measured from manually-traced lines on the microscopic images with ImageJ plug-ins (see Materials and Methods; Fig. I-3A). The mRFP fluorescent intensities tended to increase with the curvature of the interdigitated pavement cell borders (Fig. I-3B, D), suggesting that ST-mRFP accumulated at the curved apoplastic regions.

Interestingly, the ST-mRFP fluorescent intensities were low in the three-way cell wall junctions, despite their high degree of curvature (Fig. I-3C, D).

Treatment with 30 μM wortmannin, which inhibits both phosphatidylinositol 3-kinase (PI3K) and phosphatidylinositol 4-kinase (PI4K) (Jung et al. 2002), decreased both the interdigitation of pavement cells (Fig. I-4A) and ST-mRFP localization (Fig. I-4B) compared with the dimethylsulfoxide (DMSO) control. These results suggested targeted transport from Golgi bodies to the curved apoplastic regions during interdigitation of the pavement cells.

Paramural bodies were observed in leaf epidermis

To gain insight into the ultra-micro structures involved in pavement cell morphogenesis, I performed TEM observations of *Arabidopsis* leaf epidermis. The images revealed the existence of PMBs, vesicular membrane structures (30–100 nm in diameter) between the concave plasma membrane (200–800 nm in diameter) and the cell wall. PMBs existed in both sections that fixed chemically (Fig. I-5A) and by high-pressure freezing (Fig. I-5B). PMBs were more frequently observed in young leaves than in mature leaves.

Discussion

This study showed that the ST-mRFP-labeled membrane traffic pathway to apoplastic regions was involved in pavement cell morphogenesis. Additionally, the localization of ST-mRFP fluorescence suggested that targeted transport occurs from Golgi bodies to the curved apoplastic regions (Fig. I-3). ST-mRFP signals could be observed in apoplastic regions compared

to ST-GFP signals (Fig. I-S1), because mRFP are more stable than GFP at low pH (Shaner et al. 2005), as in apoplastic regions. Differences in ST-mRFP fluorescent intensities between the borders of two interdigitated cells and three-way junctions (Fig. I-3) indicated a difference in their curvature formation processes. The interdigitation of adjacent pavement cells, where ST-mRFP localized, depends on the coordinated formation of lobes and indentions. This spatially-coordinated cell expansion was considered to require extracellular auxin activate Rho-related GTPase from plants (ROPs) (Xu et al. 2010). In contrast, three-way junctions, in which ST-mRFP did not localize, resulted from cell division. Thus, pavement cell curvature resulted from coordinated cell expansion in adjacent pavement cells to which secreted ST-mRFP was targeted.

My TEM study revealed PMBs (Fig. I-5), suggesting the existence of pathways to the extracellular space via MVBs acting as exosomes in plant cells. MVBs travel to the plasma membrane, where they release the contents of their internal vesicles contents into the extracellular space by membrane fusion (Denzer et al. 2000). Such exosomes have been observed in fungi (Marchant et al. 1967) and in during animal erythrocyte maturation (Harding et al. 1983). In plants, some observations of PMBs suggested the existence of exosomes as previously reported in the pathogen defense response of *Hordeum vulgare* (An et al. 2006a, 2006b). In this study, PMBs were more frequently observed in young leaves than in mature leaves, suggesting that MVBs are involved as exosomes in pathways to the extracellular space during pavement cells morphogenesis, during which membrane and cell wall materials must be secreted into the extracellular space.

References

Abramoff MD, Magelhaes PJ, Ram SJ (2004) Image processing with ImageJ. *Biophotonics Int* 11:36–42

An Q, Ehlers K, Kogel KH, van Bel AJE, Hückelhoven R (2006a) Multivesicular compartments proliferate in susceptible and resistant MLA12-barley leaves in response to infection by the biotrophic powdery mildew fungus. *New Phytol* 172:563–576

An Q, Hückelhoven R, Kogel KH, van Bel AJE (2006b) Multivesicular bodies participate in a cell wall associated defense response in barley leaves attacked by the pathogenic powdery mildew fungus. *Cell Microbiol* 8:1009–1019

Boevink P, Oparka K, Cruz SS, Martin B, Betteridge A, Hawes C (1998) Stacks on tracks: the plant Golgi apparatus traffics on an actin/ER network. *Plant J* 15:441–447

Denzer K, Kleijmeer MJ, Heijnen HFG, Stoorvogel W, Geuze HJ (2000) Exosome: from internal vesicle of the multivesicular body to intercellular signaling device. *J Cell Sci* 113:3365–3374

Harding C, Heuser J, Stahl P (1983) Receptor-mediated endocytosis of transferrin and recycling of the transferrin receptor in rat reticulocytes. *J Cell Biol* 97:329–339

Jung JY, Kim YW, Kwak JM, Hwang JU, Young J, Schroeder JI, Hwang I, Lee Y (2002) Phosphatidylinositol 3- and 4-phosphate are required for normal stomatal movements. *Plant Cell* 14:2399–2412

Lancelle SA, Hepler PH (1992) Ultrastructure of freeze-substituted pollen tubes of *Lilium longiflorum*. *Protoplasma* 167:215–230

Latijnhouwers M, Hawes C, Carvalho C, Oparka K, Gillingham AK, Boevink P (2005) An *Arabidopsis* GRIP domain protein locates to the *trans*-Golgi and binds the small GTPase ARL1. *Plant J* 44:459–470

Marchant R, Peat A, Banbury GH (1967) The ultrastructural basis of hyphal growth. *New Phytol* 66:623–629

Naito S, Hirai MY, Chino M, Komeda Y (1994) Expression of a soybean (*Glycine max* [L.] Merr.) seed storage protein gene in transgenic *Arabidopsis thaliana* and its response to nutritional stress and to abscisic acid mutations. *Plant Physiol* 104:497–503

Nishitani K, Tominaga R (1991) In vitro molecular weight increase in xyloglucans by an apoplastic enzyme preparation from epicotyls of *Vigna angularis*. *Physiol Plant* 82:490–497

Parton RM, Fischer-Parton S, Trewavas AJ, Watahiki MK (2003) Pollen tubes exhibit regular periodic membrane trafficking events in the absence of apical extension. *J Cell Sci* 116:2707–2719

Parton RM, Fischer-Parton S, Watahiki MK, Trewavas AJ (2001) Dynamics of the apical vesicle accumulation and the rate of growth are related in individual pollen tubes. *J Cell Sci* 114:2685–2695

Robards AW, Kidwai P (1969) Vesicular involvement in differentiating plant vascular cells. *New Phytol* 68:343–349

Samalova M, Fricker M, Moore I (2006) Ratiometric fluorescence-imaging assays of plant membrane traffic using polyproteins. *Traffic* 7: 1701–1723

Samuels AL, Giddings Jr TH, Staehelin LA (1995) Cytokinesis in tobacco BY-2 and root tip cells: a new model of cell plate formation in higher plants.

J Cell Biol 130:1345–1357

Shaner NC, Steinbach PA, Tsien RY (2005) A guide to choosing fluorescent proteins. *Nat Methods* 2:905–909

Tanchak MA, Griffing LR, Mersey BG, Fowke LC (1984) Endocytosis of cationized ferritin by coated vesicles of soybean protoplasts. *Planta* 162:481–486

Toyooka K, Goto Y, Asatsuma S, Koizumi M, Mitsui T, Matsuoka K (2009) A mobile secretory vesicle cluster involved in mass transport from the Golgi to the plant cell exterior. *Plant Cell* 21:1212–1229

Xu T, Wen M, Nagawa S, Fu Y, Chen JG, Wu MJ, Perrot-Rechenmann C, Friml J, Jones AM, Yang Z (2010) Cell surface- and rho GTPase-based auxin signaling controls cellular interdigitation in *Arabidopsis*. *Cell* 143:99–110

Figures

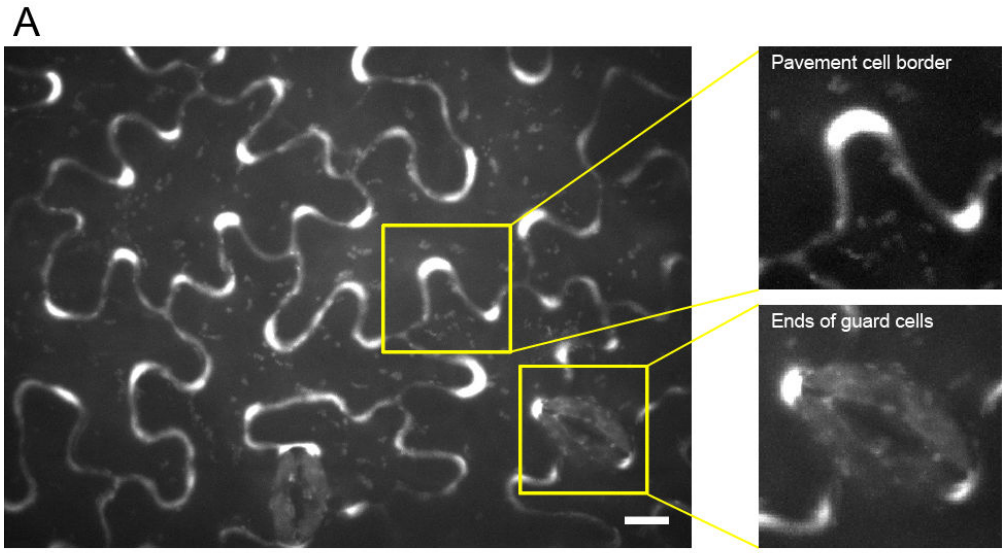

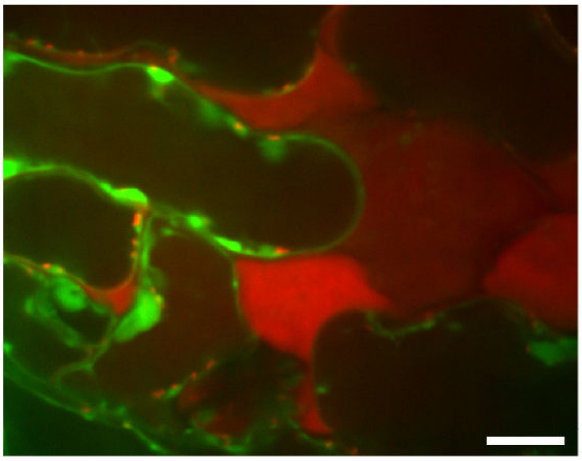

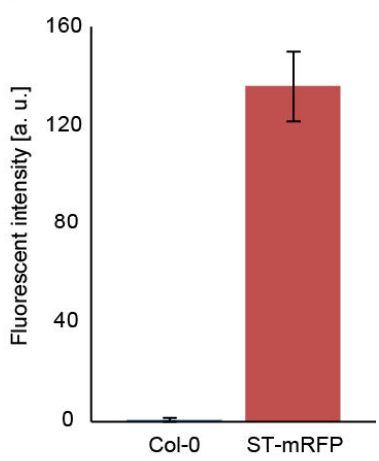

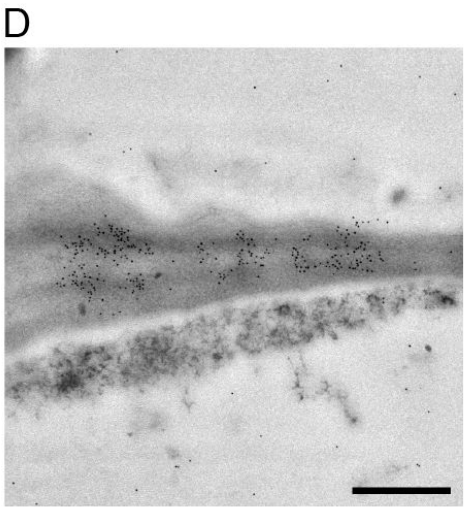

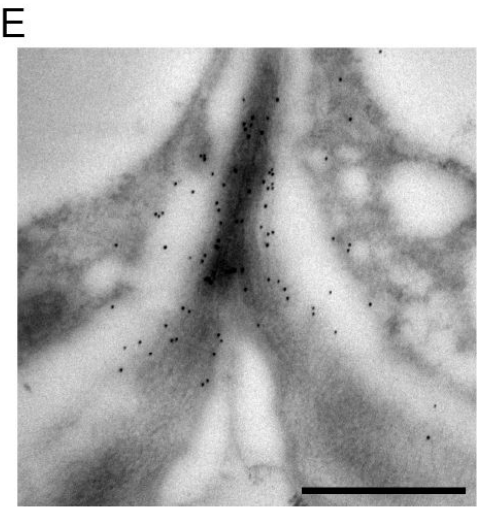

Pavement cell border

Ends of guard cells

Fig. I-1 Localizations of ST-mRFP in leaf epidermis.

(A) ST-mRFP highlighted the border of pavement cells and guard cells as well as Golgi bodies. Scale bar = 10 μm. (B) Plasmolysis of pavement cells expressing ST-mRFP. The cytoplasm was stained with 10 μg/mL FDA dye (green) under hyperosmotic condition (0.85 M NaCl) for 10 min. Note that mRFP fluorescence (red) was observed in the apoplastic regions. Scale bar = 10 μm. (C) Fluorescent intensities of mRFP in the extracted apoplast fluid. Data are mean values ± SD of 4 independent observations. (D, E) Immunogold staining of apoplastic regions with mRFP antibodies in leaves (8–10 mm in length) of 45-day-old plants expressing ST-mRFP. The pavement cell border (D) and ends of guard cells (E) were shown. Scale bars = 0.5 μm.

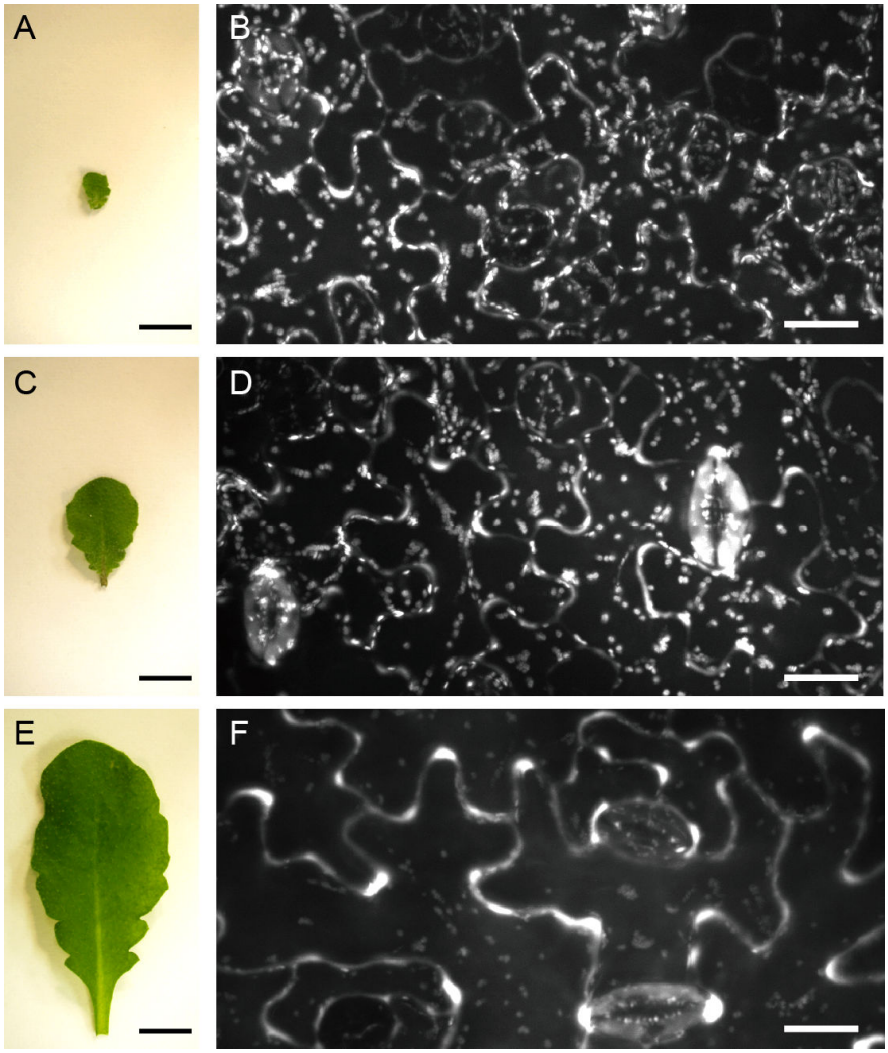

Fig. I-2　Changes of ST-mRFP localizations with leaf growth.

(A, C, E) Leaves were classified as "young leaves" (2–3 mm in length) (A), "mid-sized leaves" (8–10 mm) (C), or "mature leaves" (27–30 mm) (E). The 45-day-old plants were used for sampling. Scale bars = 5 mm. (B, D, F) Representative microscopic images of the epidermis in young leaves (B), mid-sized leaves (D), and mature leaves (F). Note that apoplastic localization of ST-mRFP became prominent during leaf growth. Scale bars = 10 μm.

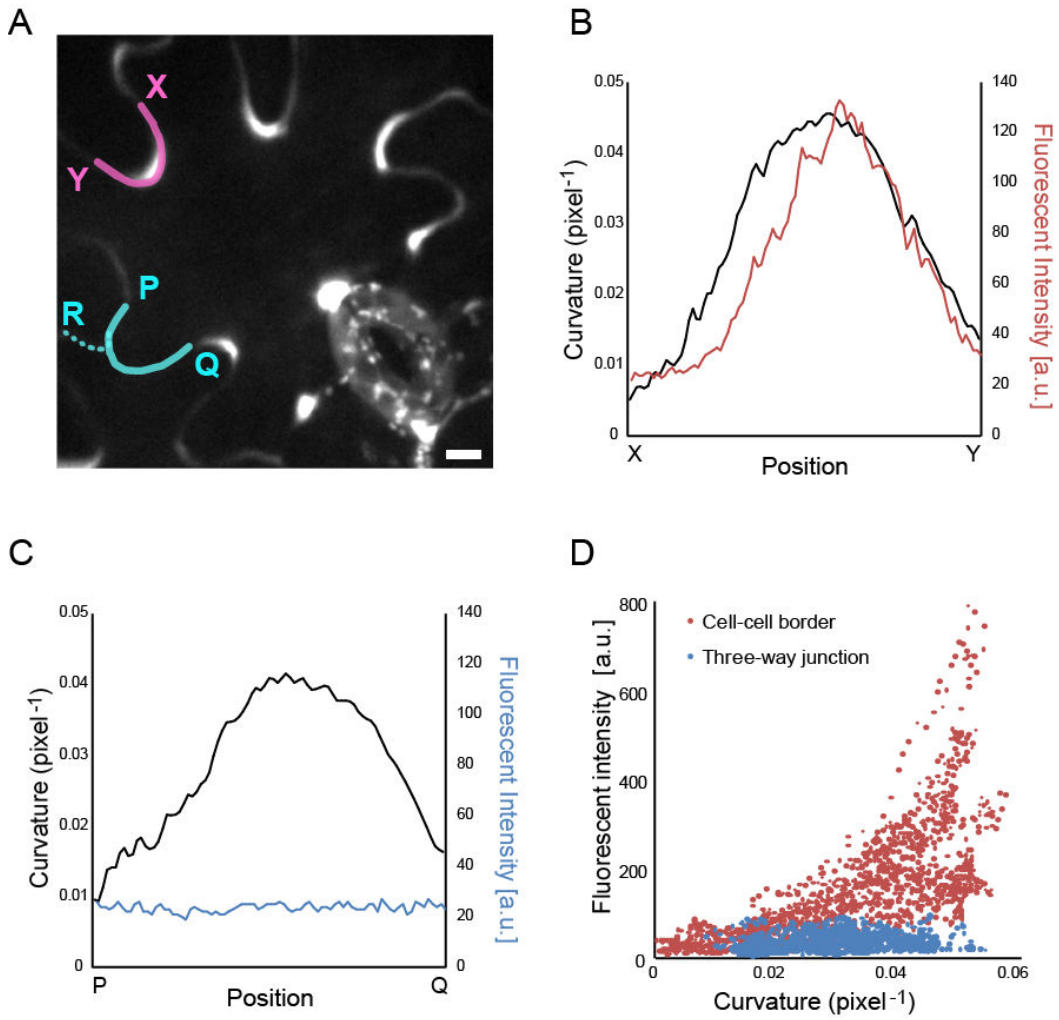

Fig. I-3 Relationship between ST-mRFP fluorescent intensity and curvature of the epidermal cell border.

(A) Representative images of ST-mRFP in leaf epidermis. The X–Y line was manually drawn along the cell border between two interdigitated pavement cells. The P–Q line was manually drawn along the cell border of a three-way cell junction (P–Q–R). Scale bar = 5 μm. (B, C) Florescent intensity profile (colored lines) and curvatures (black lines) along the X–Y axis (B) and along the P–Q axis (C) in (A). (D) A scatter plot of the mRFP fluorescent intensity and the cell border curvature. 1 pixel = 0.161 μm. I measured 1031–1368 points from independent 15 lines.

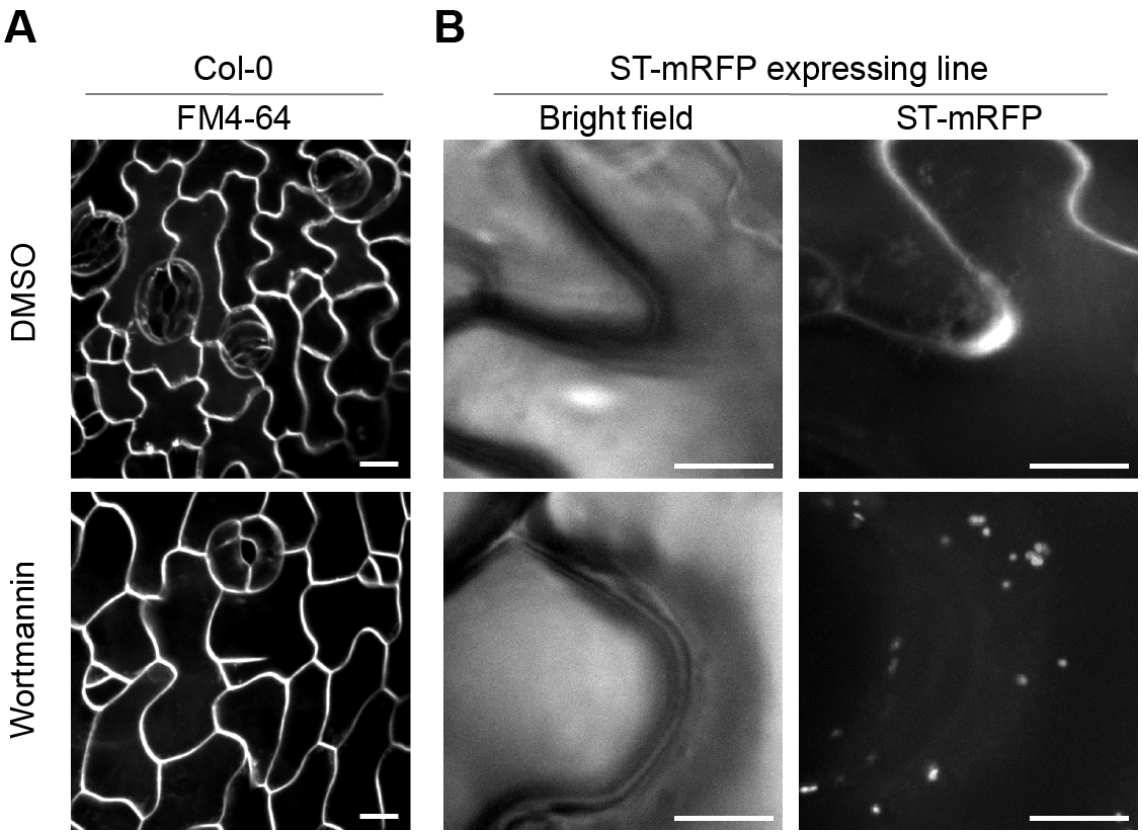

Fig. I-4 Curvature and ST-mRFP localization were sensitive to wortmannin in pavement cells.

(A, B) Representative microscopic images of leaf epidermal cells without-(top) or with-(bottom) 30 μM wortmannin. (A) Plasma membranes were stained with FM4-64 in wild-type (Col-0). (B) Effects on curvature and ST-mRFP localization in pavement cells expressing ST-mRFP. Scale bars = 10 μm.

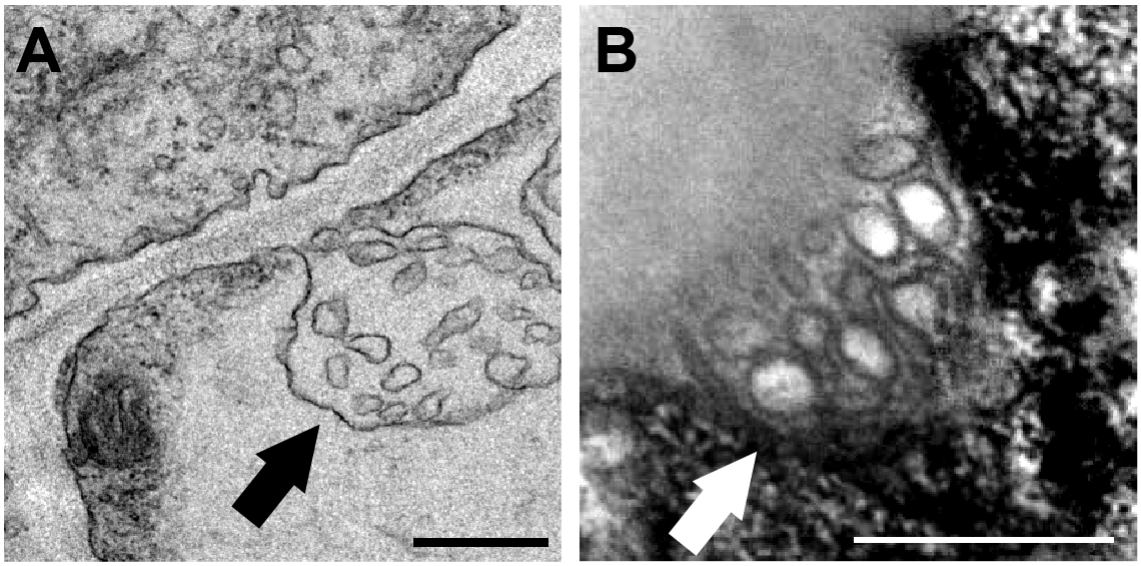

Fig. I-5　Paramural bodies in leaf epidermis.

(A, B) Electron micrographs showed paramural bodies (arrows) in pavement cells which were fixed chemically (A) or by high-pressure freezing (B). Scale bars = 500 nm.

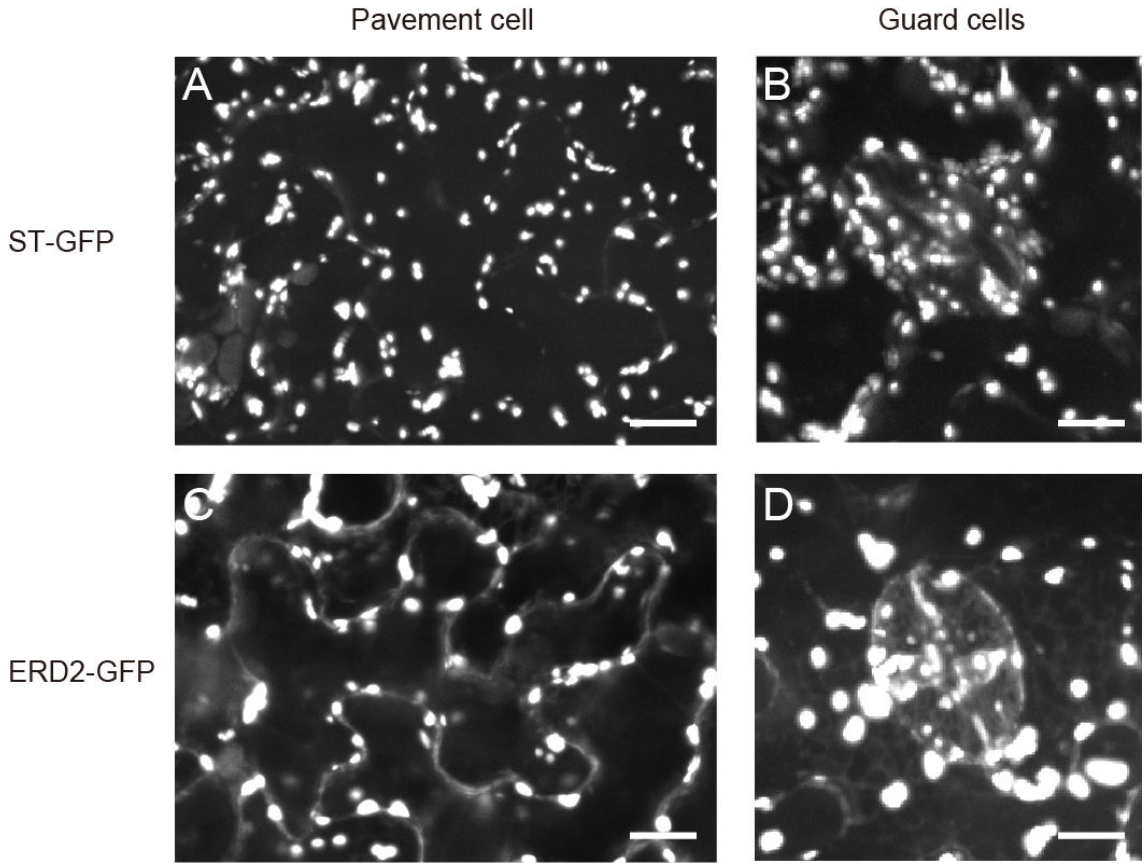

Fig. I-S1　Localizations of Golgi marker in leaf epidermis.

(A, B) ST-GFP labeled *trans*-Golgi bodies in the pavement cells (A) and the guard cells (B). (C, D) ERD2-GFP labeled *cis*-Golgi bodies in the pavement cells (C) and the guard cells (D). Scale bars = 10 μm.

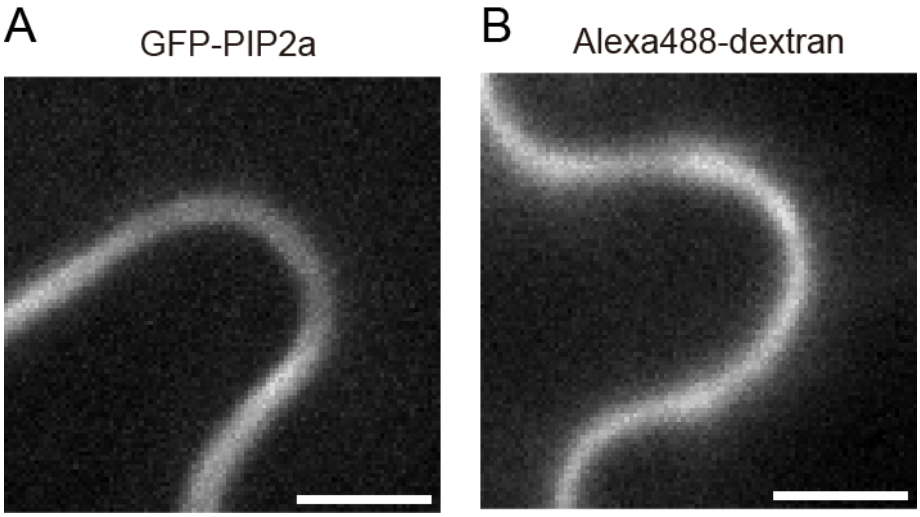

Fig. I-S2　Visualization of leaf epidermal cell borders.

(A) Plasma membranes labeled by GFP-PIP2a. (B) Apoplast stained with 1 g/L Alexa488-dextran for 4 h. Scale bars = 5 μm.

Chapter II: Role of cortical microtubule orientation in *Arabidopsis* leaf epidermis

Abstract

Leaf pavement cells are shaped like jigsaw puzzle in most dicotyledon species. Molecular genetic studies have identified several genes required for pavement cells morphogenesis and proposed that microtubules play crucial roles in interdigitation of pavement cells. In this chapter, I performed quantitative analysis on cortical microtubule orientation in *Arabidopsis* leaf pavement cells. I captured confocal images of cortical microtubules in cotyledon leaf epidermis expressing GFP-tubulinβ and quantitatively evaluated the microtubule orientations relative to the pavement cell growth axis using my original image processing techniques. My results showed that microtubules kept parallel orientations to the growth axis during pavement cell growth. In addition, I showed that immersion treatment of seed cotyledons in solutions containing tubulin polymerization and depolymerization inhibitors decreased pavement cell complexity. Treatment with oryzalin and colchicine inhibited the symmetric division of guard mother cells.

Introduction

During plant cell growth and differentiation, individual cells gradually acquire distinguishing shapes unique to their tissue types. The final cell shapes result from anisotropic cell wall deformations modulated by the cytoskeletons, especially microtubules, during cell growth. Plant cell growth patterns are roughly categorized into two classes: diffuse growth and tip growth. Diffuse growth is a major growth pattern observed in various plant cell types, and most of these cells extend preferentially along one axis. Cortical microtubules are generally aligned perpendicular to the major axis of cell elongation in diffusely growing cells. Recent studies showed that the transverse orientation of cortical microtubules was established mainly by incoming microtubules at cell edges (i.e., cross wall) (Ambrose et al. 2011, Ambrose and Wasteneys, 2012). The cortical microtubules determine the orientation of cellulose microfibrils that restrict the direction of cell expansion by guiding the movement of cellulose synthase complexes through the plasma membranes (Hasezawa and Nozaki, 1999, Paredez et al. 2006).

In contrast, tip growth is observed mainly in root hairs and pollen tubes. In this pattern of polarized cell expansion, wall extension and the incorporation of new wall material are focused at one site on the cell surface. Microtubules orient parallel to the direction of cell growth rather than transversely as in diffuse growth. The microtubules may play roles in the long distance organelle transport involved in supplying new cell walls and membranes (Cai and Cresti, 2009).

As described in Chapter I, in most dicot plants, leaf pavement cells have lobes and indentations that interlock one another like a jigsaw puzzle.

Their cell growth pattern is unlike either diffuse or tip growth because these cells have more than three growing sites (Geitmann and Ortega, 2009). Molecular genetic studies on leaf pavement cells have shown the importance of microtubules in their morphogenesis. A plant-specific member of ROPs, ROP6 activates ROP-interactive CRIB motif-containing protein 1 (RIC1) to order the microtubules and establish an indentation by restricting cell expansion locally (Fu et al. 2005, 2009). The ROP6-regulated microtubule accumulation is activated by a putative auxin receptor AUXIN BINDING PROTEIN 1 (ABP1) and the auxin efflux facilitator PINFORMED 1 (PIN1) protein (Xu et al. 2010). In the proposed model, the microtubules are rich in indentation regions but thin in lobe regions (Xu et al. 2010). However, recent observations with freeze shattering and immunolocalization or transient expression revealed that anticlinal microtubule bundles localized at expanding lobe regions, suggesting that the microtubules do not restrict cell growth but rather make lobe regions (Zhang et al. 2011). These contradictory reports indicated that the microtubules are crucial for jigsaw puzzle-shaped pavement cell morphogenesis, but their orientations and distributions are still unclear.

Using modern microscopic image analysis techniques to quantitatively evaluate cytoskeletal organization (e.g., Higaki et al. 2010, Yoneda et al. 2007, 2010) would help our understanding of the structural changes and physiological roles of microtubules during pavement cell growth. In this chapter, I captured GFP-labeled cortical microtubules in *Arabidopsis* cotyledon pavement cells of various sizes and quantitatively evaluated the microtubule orientations in pavement cells with multiple cell growth directions.

Materials and Methods

Plant materials and growth conditions

Seeds of transgenic *Arabidopsis thaliana* plants expressing GFP-tubulinβ (Abe and Hashimoto, 2005) were kindly provided by Prof. Takashi Hashimoto (Nara Institute of Science and Technology). *Arabidopsis* plants were grown on 1/2 Murashige–Skoog [2.3 mg L^{-1} Murashige and Skoog Plant Salt Mixture (Code No. 392-00591: Wako Pure Chemical Industries, Osaka, Japan)] (pH 5.8) gellan gum plates in growth chambers at 23.5°C with 60% relative humidity and a 12 h light/12 h dark cycle, using 100 μmol m^{-2} s^{-1} white lights.

Microscopy

To acquire confocal images, I used a fluorescence microscope (IX-71; Olympus, Tokyo, Japan) equipped with a confocal laser scanning head and control system (FLUOVIEW FV300; Olympus), together with a sapphire laser (488 nm; Showa Optronics, Tokyo, Japan) and a helium-neon laser (543 nm; Showa Optronics). At image acquisition, pixel width (0.36 μm) was fixed.

Evaluation of microscopic images

The cell region was selected by manually tracing, and the cell areas and perimeters were measured with ImageJ software (Abramoff et al. 2004) using the "Analyze – Measure" menu. Cell complexity was defined as

$$Complexity = \frac{Perimeter^2}{4\pi \cdot Area}$$

To preprocess the quantitative evaluations of microtubule orientations, the maximum intensity projections were constructed from 0.5 μm-interval serial optical sections (Fig. II-S1, Raw image). From the projection image, microtubules were extracted by "Plugins-kbi-KbiFilter2d-LineFilters-lineExtract". The KBI plug-in package can be downloaded for free from http://hasezawa.ib.k.u-tokyo.ac.jp/zp/Kbi/ImageJKbiPlugins. The cell medial axis was obtained from a manually-segmented cell region image (Fig. II-S1, Cell region image) using the ImageJ menu "Process – Binary – Skeletonize" (Fig. II-S1, Cell medial axis image).

To evaluate microtubule orientations, I measured the mean angular difference between microtubule pixel pairs and the nearest segments of the cell medial axis in the processed images (Fig. II-1D) essentially as previously described (Higaki et al. 2010, Yoneda et al. 2007, 2010) using Kbi plug-in and the ImageJ menu "Plugins-kbi-Kbi_IjTool-epidermalAnalysis". The mean angular difference $\Delta\theta$ was defined by

$$\Delta\theta = \frac{1}{N}\sum_{i=1}^{N} D(i) \qquad (1)$$

$$D(i) = \begin{cases} \left|\theta_{MT}^{i} - \theta_{CMAedge}^{i}\right| & if \ \left|\theta_{MT}^{i} - \theta_{CMAedge}^{i}\right| \le 90^{\circ} \\ \left|\theta_{MT}^{i} - \theta_{CMAedge}^{i}\right| - 90^{\circ} & if \ \left|\theta_{MT}^{i} - \theta_{CMAedge}^{i}\right| > 90^{\circ} \end{cases} \qquad (2)$$

where N, θ_{MT}^{i} and $\theta_{CMAedge}^{i}$ are the number of microtubule segments

i-th angles of microtubule segments (1.4 μm correspond 4 pixels), and segments of the nearest cell medial axis, respectively. *MT* and *CMAedge* indicate microtubule and cell medial axis, respectively.

FM4-64 staining

To visualize plasma membrane, cells were stained with 32 μM FM4-64 dye (Life Technologies, Tokyo, Japan) in basal buffer [5mM MES-Tris, 10 mM $CaCl_2$, 50 mM KCl, pH6.5] at room temperature for 5–10 min.

Inhibitor treatments

In a 96-well plate (Sumilon Multi Well Plate; Sumitomo Bakelite, Tokyo, Japan), *Arabidopsis* seeds (wild type (Col-0), GFP-tubulinβ expressing line, or enhancer trap line E1728 (Gardner et al. 2009)) were germinated in distilled water containing inhibitors. The seedlings were treated with 6 μM propyzamide (Sigma-Aldrich Japan, Tokyo, Japan), 50 μM colchicine (Sigma-Aldrich Japan), 10 μM oryzalin (Wako Pure Chemicals, Tokyo, Japan), or 30 μM taxol (Tocris Bioscience, MO, U.S.A.) for 7 days, and then observed.

Results

Cortical microtubules tended to be oriented parallel to cell medial axis in pavement cells

To evaluate the cortical microtubule changes during pavement cell growth, surfaces of *Arabidopsis* cotyledon leaves expressing GFP-tubulinβ were observed 3–12 day after germination (DAG) using CLSM. I manually segmented 166 pavement cell regions (Fig. II-S1, Raw image to Cell region

image) from the microscopic fluorescent images. The pavement cell area and cell complexity were measured. Cell complexity was proportional to cell area in the 3–12 DAG cotyledons (Fig. II-1A, B), suggesting that pavement cell morphogenesis occurred during this period.

Next, I evaluated the relationship between the pavement cell growth axis and microtubule orientation. To evaluate the direction of cell growth, cell medial axis was obtained from the binarized cell region image by skeletonization (Fig. II-S1, Cell region image to Cell medial axis image). In addition, I skeletonized microtubules from GFP-tubulinβ images (white lines in Fig. II-1D) and measured the mean angular differences ($\Delta\theta$) from the nearest part of the medial axis (cyan lines in Fig. II-1D) of each cell as a numeric indicator of microtubule orientation relative to the cell growth axis (Fig. II-1C, D). When microtubules are oriented parallel or transversely to the cell medial axis, $\Delta\theta$ is less than or more than 45.0°, respectively. When the microtubules are randomly oriented, $\Delta\theta$ is approximately 45.0°. My measurements from the pavement cell image dataset showed that $\Delta\theta$ displayed great variation (SD = 7.13) in simply-shaped cells with lower cell complexity (from 1 to 3) than in more complexly-shaped cells (complexity from 6 to 8; (SD = 3.03). The median value of $\Delta\theta$ increased with cell complexity from 37.9° in cells with complexity of 1–3 to 41.8° in cells with complexity of 6–8. A similar trend was found in the minimum values of $\Delta\theta$ (23.0° when complexity was 1–3; 36.8° when complexity was 6–8). Importantly, the median values of $\Delta\theta$ did not exceed 45.0° in my observations (Fig. II-1C, D), suggesting that the cortical microtubules oriented rather parallel to the cell growth axis. Moreover, in complicated cells with $\Delta\theta$ around 45.0°, cortical microtubules showed parallel orientations in some

local regions (Fig. II-1B, D the largest cell).

Treatment with microtubule inhibitors deformed pavement cells and guard cells

To study the roles of microtubules in leaf epidermal cell morphogenesis, *Arabidopsis* seeds were immersed into water containing 0.1% DMSO or microtubule inhibitors, and cotyledons were allowed to expand 7 day after treatment. The effects of inhibitors on microtubules were checked using GFP-tubulinβ (Fig. II-2A, GFP-tubulinβ). The cell shapes were visualized by staining the plasma membrane with FM4-64 (Fig. II-2A, FM4-64). In DMSO control cotyledons, pavement cells had normal lobed and indented regions (Fig. II-2A, DMSO). Treatment with tubulin polymerization inhibitors decreased cell complexity relative to the control (Fig. II-2A and B, Propyzamide, Colchicine, and Oryzalin). Propyzamide and oryzalin significantly decreased cell area (Fig. II-2C), suggesting that they affected cell growth itself. Propyzamide induced abnormally-shaped stomata that had a distorted plane of division (Fig. II-2A, Propyzamide). In the colchicine and oryzalin treatments, number of stomata decreased but many circular cells appeared (Fig. II-2A, Colchicine and Oryzalin). When I observed the colchicine- or oryzalin-treated cotyledons of the GAL4 GFP enhancer trap line E1728, in which mature guard cells are specified by GFP fusions with an endoplasmic reticulum (ER) retention signal (Gardner et al. 2009), GFP signals were clearly detected in the circular cells (Fig. II-2D). Therefore, these circular cells probably progress into mature guard cells, suggesting that symmetric division of guard mother cells was inhibited by colchicine and oryzalin. Treatment with taxol, a tubulin depolymerization inhibitor, significantly decreased cell complexity but did not affect cell area and guard

mother cell division (Fig. 2A–C, Taxol). These results suggested that both tubulin polymerization and depolymerization are crucial to pavement cell morphogenesis. To make normal stomata via symmetric division of guard mother cells, tubulin polymerization is also required.

Discussion

Based on my quantitative evaluation, I propose three stages of microtubule orientation with respect to the pavement cell growth axis. First, in immature cells with complexity less than 3, cortical microtubules are mostly aligned with the cell growth axis but their orientations vary greatly. In early stage of pavement cell morphogenesis, ROP6-dependent microtubule reorientation often occurs at various sites along the cell periphery (Fu et al. 2005, 2009, Xu et al. 2010). In my quantification, the microtubule reorientations may be a variety with high $\Delta\theta$.

Second, in expanding cells with complexity of 3 to 6, the cortical microtubules orient parallel to the cell growth axis, as in tip growth but not diffuse growth. Previous molecular genetic studies showed that pavement cell growth was modulated by ROP signaling in is tip growth (Fu et al. 2005, 2009). However, expanding cell edges acted as barriers to microtubules by inducing incoming microtubules in an "edge effect" (Ambrose et al. 2011). Using computational simulations of microtubule dynamics, Prof. Wasteneys' group proposed that the transverse orientations of microtubules were spontaneously formed in diffuse-growing plant cells, which have two expanding edges, as a result of self-organizational mechanisms (Ambrose et

al. 2011, Ambrose and Wasteneys, 2012). If the anticlinal cell faces between adjacent cells are sharp edge, microtubule orient as in tip growth by self-organization.

Third, in mature cells with complexity more than 6, the parallel cortical microtubules are located in sub-regions of the cells, but their orientations are less directly linked to the cell growth axis, as shown by their $\Delta\theta$ near 45.0°. This tendency suggested that cortical microtubule self-organization occurred in different regions of complex pavement cells that had expanded sufficiently, resulting in multiple parallel domains as previously proposed by Ambrose and Wasteneys (2012).

In this chapter, I also showed the effects of microtubule inhibitors on pavement cell morphogenesis (Fig. II-2). Treatment with tubulin polymerization and depolymerization inhibitors decreased cell complexity, suggesting that both polymerization and depolymerization are crucial to pavement cell morphogenesis. It was repoted that both overexpressing or knockdown of *microtubule-associated proteins18 (MAP18)* coding for a microtubule destabilizing protein resulted in simpler pavement cell morphology (Wang et al. 2007), supporting my pharmacological results. In the case of tubulin polymerization inhibitors, propyzamide induced abnormally-shaped stomata, and colchicine and oryzalin inhibited symmetric division of guard mother cells. In contrast, division of pavement cells or asymmetric division of meristemoid mother cell was not disturbed by these inhibitors. A previous study showed that colchicine also inhibited guard mother cell division in *Zea maize* (Panteris et al. 2007). When γ-tubulin complex protein expression was repressed by amiRNA, cell division of guard mother cells was inhibited (Kong et al. 2010). The division and

differentiation of guard mother cells to guard cells are regulated by a transcription factor FAMA and distinctly different from other cell divisions (Ohashi-Ito and Bergmann, 2006). These results suggested that symmetric division of guard mother cells is sensitive to colchicine and oryzalin. These inhibitors potentially affect the mitotic spindle and phragmoplast, which may have lower stability in guard mother cells than in pavement cells or meristemoid cells.

References

Abe T, Hashimoto T (2005) Altered microtubule dynamics by expression of modified alpha-tubulin protein causes right-handed helical growth in transgenic *Arabidopsis* plants. *Plant J* 43:191–204

Abramoff MD, Magelhaes PJ, Ram SJ (2004) Image processing with ImageJ. *Biophotonics Int* 11:36–42

Ambrose C, Allard JF, Cytrynbaum EN, Wasteneys GO (2011) A CLASP-modulated cell edge barrier mechanism drives cell-wide cortical microtubule organization in *Arabidopsis*. *Nat Commun* 16:430

Ambrose C, Wasteneys GO (2012) Nanoscale and geometric influences on the microtubule cytoskeleton in plants: thinking inside and outside the box. *Protoplasma* 249:S69–76

Cai G, Cresti M (2009) Organelle motility in the pollen tube: a tale of 20 years. *J Exp Bot* 60:495–508

Fu Y, Gu Y, Zheng Z, Wasteneys G, Yang Z (2005) *Arabidopsis* interdigitating cell growth requires two antagonistic pathways with opposing action on

cell morphogenesis. *Cell* 120:687–700

Fu Y, Xu T, Zhu L, Wen M, Yang Z (2009) A ROP GTPase signaling pathway controls cortical microtubule ordering and cell expansion in *Arabidopsis*. *Curr Biol* 19:1827–1832

Gardner MJ, Baker AJ, Assie JM, Poethig RS, Haseloff JP, Webb AA (2009) GAL4 GFP enhancer trap lines for analysis of stomatal guard cell development and gene expression. *J Exp Bot* 60:213–226

Geitmann A, Ortega JK (2009) Mechanics and modeling of plant cell growth. *Trends Plant Sci* 14:467–478

Hasezawa S, Nozaki H (1999) Role of cortical microtubules in the orientation of cellulose microfibril deposition in higher-plant cells. *Protoplasma* 209:98–104

Higaki T, Kutsuna N, Sano T, Kondo N, Hasezawa S (2010) Quantification and cluster analysis of actin cytoskeletal structures in plant cells: role of actin bundling in stomatal movement during diurnal cycles in *Arabidopsis* guard cells. *Plant J* 61:156–165

Kong Z, Hotta T, Lee YR, Horio T, Liu B (2010) The γ-tubulin complex protein GCP4 is required for organizing functional microtubule arrays in *Arabidopsis thaliana*. *Plant Cell* 22:191–204

Ohashi-Ito K, Bergmann DC (2006) *Arabidopsis* FAMA controls the final proliferation/differentiation switch during stomatal development. *Plant Cell* 18:2493–2505

Panteris E, Galatis B, Quader H, Apostolakos P (2007) Cortical actin filament organization in developing and functioning stomatal complexes of *Zea mays* and *Triticum turgidum*. *Cell Motil Cytoskeleton* 64:531–548

Paredez AR, Somerville CR, Ehrhardt DW (2006) Visualization of cellulose

synthase demonstrates functional association with microtubules. *Science* 312:1491–1495

Wang X, Zhu L, Liu B, Wang C, Jin L, Zhao Q, Yuan M (2007) *Arabidopsis* MICROTUBULE-ASSOCIATED PROTEIN18 functions in directional cell growth by destabilizing cortical microtubules. *Plant Cell* 19:877–889

Xu T, Wen M, Nagawa S, Fu Y, Chen JG, Wu MJ, Perrot-Rechenmann C, Friml J, Jones AM, Yang Z (2010) Cell surface- and rho GTPase-based auxin signaling controls cellular interdigitation in *Arabidopsis*. *Cell* 143:99–110

Yoneda A, Higaki T, Kutsuna N, Kondo Y, Osada H, Hasezawa S, Matsui M (2007) Chemical genetic screening identifies a novel inhibitor of parallel alignment of cortical microtubules and cellulose microfibrils. *Plant Cell Physiol* 48:1393–1403

Yoneda A, Ito T, Higaki T, Kutsuna N, Saito T, Ishimizu T, Osada H, Hasezawa S, Matsui M, Demura T (2010) Cobtorin target analysis reveals that pectin functions in the deposition of cellulose microfibrils in parallel with cortical microtubules. *Plant J* 64:657–667

Zhang C, Halsey LE, Szymanski DB (2011) The development and geometry of shape change in *Arabidopsis thaliana* cotyledon pavement cells. *BMC Plant Biol* 11:27

Figures

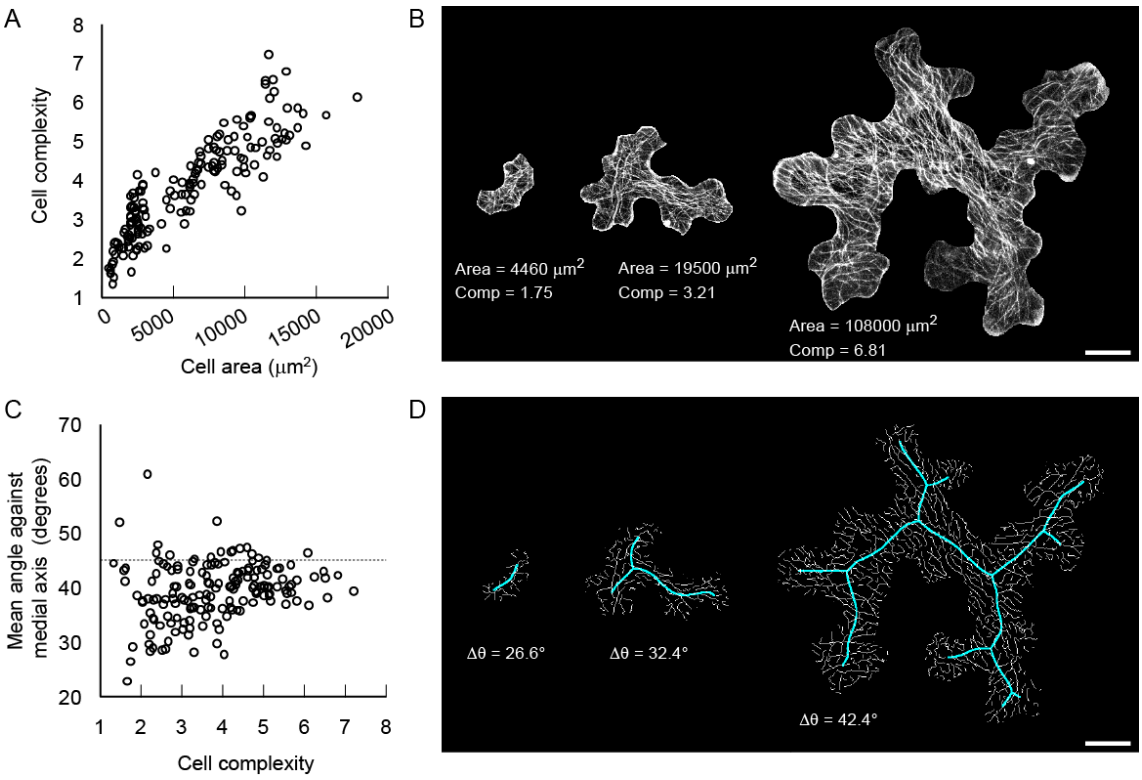

Fig. II-1 Measurement of microtubule orientations during pavement cell growth in *Arabidopsis* leaf expressing GFP-tubulinβ.

(A) A scatter plot of cell area and cell complexity. (B) Representative images of GFP-tubulinβ in pavement cells. Area and Comp indicate cell area or cell complexity, respectively. (C) A scatter plot of cell complexity and mean angle against medial cell axis (degrees). Dotted line indicates 45.0°. (D) Merged images of extracted microtubules (white) and skeletonized cell medial axis (cyan) of the cells shown in (B). $\Delta\theta$ represents mean angle against medial axis (degrees). N = 166 cells. Scale bars = 10 μm.

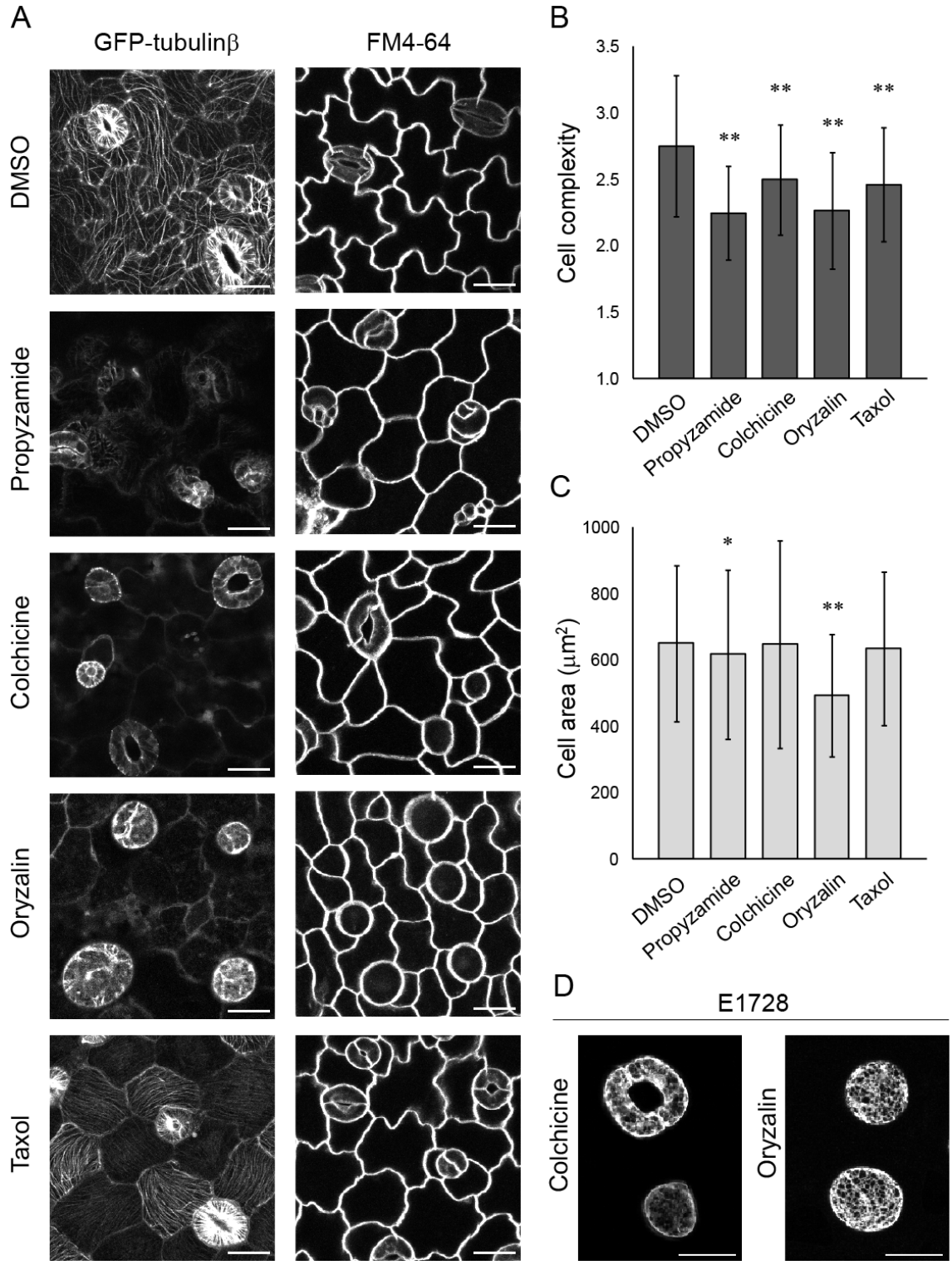
A
GFP-tubulinβ
FM4-64
DMSO
Propyzamide
Colchicine
Oryzalin
Taxol
B
Cell complexity
3.5
3.0
2.5
2.0
1.5
1.0
**
**
**
**
DMSO
Propyzamide
Colchicine
Oryzalin
Taxol
C
Cell area (μm²)
1000
800
600
400
200
0
*
**
DMSO
Propyzamide
Colchicine
Oryzalin
Taxol
D
E1728
Colchicine
Oryzalin

Fig. II-2　Effects of microtubule inhibitors on leaf epidermal cell morphology and growth.

(A) Representative microscopic images of inhibitor-treated leaf epidermal cells. (Left) Microtubules were labeled by GFP-tubulinβ. (Right) Plasma membranes were stained with FM4-64 in wild-type (Col-0). (B, C) Effects of treatment with inhibitors on pavement cell complexities (B) and cell areas (C) in wild-type (Col-0). N = 511–829 cells. Data are means ± SD of pavement cells. Significances compared with DMSO control were determined using the Student's t-test. *p*-value *< 0.05, **<0.01. (D) Leaf epidermis in enhancer trap line E1728 in which mature guard cells were labeled with GFP fusions with ER retention signal (Gardner et al. 2009). Note that the circle shaped cells were clearly labeled with GFP. Scale bars = 20 μm.

Fig. II-S1　Image processing for determination of cell medial axis.

In order to evaluate the direction of cell growth, maximum intensity projections were constructed from serial optical sections (Raw image), and cell shapes were selected and binalized (Cell region image). Cell medial axes were obtained from cell region image by skeletonization (Cell medial axis image). See also Materials and Methods.

Chapter III: Sugar solution immersion affects on *Arabidopsis* stomatal distribution

Abstract

The spatial distribution of plant stomata is a model system to study epidermal cell pattern formation. Molecular genetic approaches have identified several key genes required for stomatal distribution patterning, but external conditions that perturb the stomatal spacing distribution have not yet been identified. I found that immersing hydroponic cultures in 1–5% sucrose solution induced abnormally clustered stomata in the cotyledons of *Arabidopsis* seedlings. Clustered stomata were also induced by treatment with glucose or fructose solution but not by mannitol solution, suggesting that osmotic stress was not a cause of the disturbed stomatal patterns. Stomatal lineage cell-specific enhancer trap lines revealed that the sugar solution treatment led to ectopic expression of stomatal lineage cell-specific genes in non-stomatal lineage cells. Aniline blue staining also showed that there was reduced deposition of callose, a plant cell wall component, in new cell walls during formation of stomatal precursor cells (meristemoids). These results suggested that the immersion treatment with sugar solution permitted ectopic guard cell differentiation through dysfunction of the cell wall dividing stomatal- and non-stomatal lineage cells. My simple induction system for clustered stomata provides a suitable tool for further studies to investigate the one-cell-spacing rule during plant stomatal development (Akita et al. 2013).

Introduction

Plant stomata are pores enabling gas exchange and transpiration on the aerial plant body surface that are formed by a pair of kidney-shaped epidermal cells named guard cells. There are very few guard cell pairs in direct contact with one another, and the spatial regularity of these differentiated cells is known as the "one-cell-spacing rule" (Sachs, 1991). This one-cell-spacing rule is thought to help ion and/or water exchange between guard cells and neighboring epidermal cells during stomatal movement. Screening of *Arabidopsis* stomatal distribution mutants has identified several genes that positively or negatively regulate guard cell differentiation. Gene identification and functional analysis has suggested that guard cell differentiation is negatively regulated by EPIDERMAL PATTERNING FACTORs (EPFs) (Hara et al. 2007, 2009), which are putative ligand peptides secreted from stomatal lineage cells, in cooperation with the putative receptor TOO MANY MOUTHS (TMM) (Yang and Sack, 1995, Geisler et al. 2000) or ERECTA-family leucine-rich-repeat receptor-like kinases (Shpak et al. 2005). Downstream MAPK cascades including YODA (MAPKKK) (Bergmann et al. 2004), MKK4/5 (MAPKK) (Wang et al. 2007) and MPK3/6 (MAPK) (Wang et al. 2007) inactivate the heterodimeric transcription factor SPEECHLESS (SPCH)/ SCREAM (SCRM) (MacAlister et al. 2007, Kanaoka et al. 2008) or MUTE/SCRM (Pillitteri et al. 2007, Kanaoka et al. 2008) that positively regulates guard cell differentiation. A positive regulator of guard cell differentiation STOMAGEN/EPFL9, a secreted peptide from mesophyll cells, has been identified (Sugano et al. 2010, Kondo et al. 2010). It is also suggested that there is an intrinsic

mechanism to ensure appropriate spacing. BREAKING OF ASYMMETRY IN THE STOMATAL LINEAGE (BASL) is an essential regulator of the unequal cell division that separates stomatal lineage cells and non-stomatal lineage cells with cell periphery localization distal to the unequal division plane, that is, dysfunction of BASL results in direct contact between stomatal precursor cells, meristemoids, and the subsequent guard cells (Dong et al. 2009). The localization and functions of BASL in unequal cell division plane determination is independent of putative ligands for stomatal-derived signaling, TMM or EPF1 (Dong et al. 2009). In addition, cell wall integrity is also suggested to be important for the one-cell-spacing rule. GLUCAN SYNTHASE-LIKE 8 (GSL8)/CHORUS (CHOR) is a putative synthase of callose, which is a homopolysaccharide that is abundant in the cell plate and new cell wall during plant cytokinesis (Chen et al. 2009, Guseman et al. 2010). Dysfunction of GSL8/CHOR leads to stomatal clusters in direct contact, implicating the leakage of cell fate determinants or other regulatory factors (Guseman et al. 2010).

As described above, mutant studies have given us the molecular basis for plant stomatal spacing patterns. However, as far as I know, there have been no reports about conditions or treatments of non-gene products that disturb the stomatal one-cell-spacing rule. I believe that establishment of an experimental system to perturb the one-cell-spacing rule would also promote my knowledge of plant stomatal pattern formation. In this chapter, I report that sugar solution immersion induces clustered stomata in *Arabidopsis* seedlings, and discuss its implications.

Materials and Methods

Plant growth conditions

Sterilized *Arabidopsis thaliana* wild-type seeds (Col-0) or enhancer trap lines E1728 and E1627 (Gardner et al. 2009) were grown in 1/2 Murashige-Skoog media solution [2.3 mg L^{-1} Murashige and Skoog Plant Salt Mixture (Code No. 392-00591: Wako Pure Chemical Industries, Osaka, Japan)] (pH 5.8) supplemented with or without sucrose (Code No. 193-00025: Wako Pure Chemical Industries), glucose (Code No. 049-31165: Wako Pure Chemical Industries), fructose (Code No. 127-02765: Wako Pure Chemical Industries) or mannitol (Code No. 130-00855: Wako Pure Chemical Industries) using a 24-well plate (Sumilon Multi Well Plate, Sumitomo Bakelite, Tokyo, Japan) in a growth chamber at 23.5°C with a 12 h light/12 h dark cycle (100 μmol m^{-2} s^{-1} white light).

Cell staining

To visualize plasma membranes, leaves were immersed in basal buffer [5 mM MES-Tris, 10 mM $CaCl_2$, 50 mM KCl, pH6.5] supplemented with 32 μM FM4-64 (Life Technologies, Tokyo, Japan) for 10 min. For callose staining, 4-day-old seedlings were immersed in basal buffer supplemented with 0.02% (w/v) aniline blue for 1 week at 4°C (Kuwabara et al. 2011).

Microscopy and image analysis

To acquire confocal images, I used a fluorescence microscope (IX-71; Olympus, Tokyo, Japan) equipped with a confocal laser scanning head and control system (FLUOVIEW FV300; Olympus), together with a sapphire laser (488 nm; Showa Optronics, Tokyo, Japan) and a helium-neon laser (543

nm; Showa Optronics). Maximum intensity projection images were reconstructed from serial optical sections obtained at 0.5 μm intervals with the ImageJ software. The clustered stomata were manually counted using the ImageJ interface. To detect the fluorescence from aniline blue, I used a fluorescence microscope (BX; Olympus) equipped with a CCD camera system (DP70; Olympus).

Results

Sugar solution immersion affects stomatal distribution

Sterilized *Arabidopsis* seeds were sowed in a 24-well plate filled with sugar-free, 3% sucrose, glucose, fructose and mannitol solutions to immerse the emerged cotyledons. The sugar solution treatment enhanced seedling growth and thickened the cotyledons of 12- to 15-day-old seedlings (Fig. III-1A). Visualization of plasma membranes of the cotyledon epidermis with the fluorescent dye FM4-64 showed that clustered stomata were frequent in the seedlings immersed in 3% sucrose, glucose or fructose (Fig. III-1B). In the cotyledon epidermis of seedlings immersed in 1–5% sucrose solution, stomatal pairs (16.3–22.0%), trios (7.36–12.1%), quartets (6.67–3.90%) and clusters of 5–12 adjacent stomata (6.31–4.76%) were observed (Fig. III-2A). Comparable stomata frequencies were confirmed in the glucose and fructose treatments (Fig. III-2B), and there were highly significant differences with sugar-free conditions (p-value < 0.0001, Mann–Whitney's U-test). The stomatal density also significantly increased about 2–3 times after sucrose, fructose or glucose solution immersion compared with sugar-free conditions (Fig. III-S1). The clustered stomata were also induced in true leaves

immersed in 3% sucrose solution (Fig. III-S2A). Clustered stomata on cotyledons were rarely observed in sugar-free control conditions (Fig. III-1B and III-2A, Sugar-free) or 3% mannitol solution (Fig. III-1B and III-2B, 3% mannitol). These results suggested that clustered stomata formation was not a result of osmotic effects. In the cotyledon epidermis of seedlings grown on a gellan gum plate supplemented with 3% sucrose, the stomata were very rarely clustered (Fig. III-S2B). This observation suggested that direct exposure of the cotyledon epidermis to the solution was required for sugar-induced breaking of the stomatal one-cell-spacing rule.

Callose deposition in cell plates was perturbed by sugar solution immersion

To check whether the clustered kidney-shaped cells genetically progressed into mature guard cells, I next observed the cotyledons of the GAL4 GFP enhancer trap line E1728, in which mature guard cells are specifically labeled by GFP with an ER-retention signal (Gardner et al. 2009, Higaki et al. 2012). In the sucrose treatment, the clustered cells showed variations in size but GFP signals were clearly detected (Fig. III-3B); GFP signals were also detected in the no sugar treatment (Fig. III-3A). The enhancer trap line E1627 labels stomatal lineage cells including meristemoids, guard mother cells and guard cells (Gardner et al. 2009) (Fig. III-3C). Interestingly, E1627 labeled the jigsaw puzzle-shaped epidermal cells in sucrose-treated cotyledon epidermis (Fig. III-3D), with a cigar-shaped ER-body (an ER-derived structure) (Matsushima et al. 2003). In the control sugar-free solutions, the jigsaw puzzle-shaped epidermal cells were never labeled with GFP-ER in the E1627 line (Fig. III-3C).

Thus, I next investigated the effects of sugar solution immersion on

callose deposition in newly synthesized cell walls in the cotyledon epidermis by aniline blue staining (Kuwabara et al. 2011). To efficiently observe new cell walls, younger 4-day-old seedlings were used (Fig. III-S3). Aniline blue fluorescence was clearly detected from new cell walls separating meristemoids and epidermal cells in the control (Fig. III-4A). However, I could not detect significant fluorescence from aniline blue in new cell walls of samples treated with sucrose solution (Fig. III-4B).

Discussion

In this chapter, I found that sucrose solution immersion induced clustered stomatal distributions with abnormal gene expression pattern in E1627 line (Fig. III-2, 3). These results suggested that sucrose treatment conferred the jigsaw puzzle-shaped epidermal cells with stomatal lineage-like gene expression patterns. This feature suggests a working hypothesis that sugar solution immersion induces leakage of unidentified guard cell-fate determinants into non-stomatal lineage cells, much like in a previous report on *gsl8/chor* mutants that showed similar clustered stomata phenotypes (Guseman et al. 2010). GSL8/CHOR was suggested to positively regulate callose synthesis at the expanding cell plate, because reduced callose deposition was observed at the new cell wall in the *gsl8/chor* mutant (Chen et al. 2009, Gusemen et al. 2010). New cell walls with reduced callose have been suggested to be unable to contain cell-fate determinants in stomatal lineage cells (Guseman et al. 2010).

Decreased fluorescence of aniline blue in new cell walls suggested

that immersion in sugar solution suppresses callose deposition during unequal cell division in the cotyledon epidermis as previously reported in the *gsl8/chor* mutant (Chen et al. 2009, Gusemen et al. 2010). One possible reason why sugar treatment results in reduced callose deposition is substrate inhibition of sucrose synthase (SuSy). It has been suggested that a kind of SuSy is coexpressed with callose synthase and catalyzes the reversible conversion of sucrose and uridine diphosphate (UDP) to UDP-glucose and fructose, supplying UDP-glucose for synthesis of cell wall components including callose (Amor et al. 1995, Barratt et al. 2011). SuSy is reported to be inhibited in the UDP-glucose synthetic direction by high concentrations of the substrate fructose or UDP-glucose (Barratt et al. 2001, Bieniawska et al. 2007). In my experimental system, immersion in sugar solutions might possibly have induced substrate inhibition of UDP-glucose producing SuSy activity *in vivo*, but further studies are necessary to clarify the relationship between carbohydrate metabolism and the establishment of the stomatal one-cell-spacing rule.

In conclusion, I have established an experimental system for reproducible induction of clustered stomata in *Arabidopsis* seedlings by immersion into sucrose, glucose or fructose solution. Sugar solution immersion reduced callose deposition during the unequal cell division that separates stomatal lineage cells and nonstomatal lineage cells, and the compromised cell wall integrity might result in guard cell-fate determinant leakage and clustered stomata. This easy hydroponic culture system using sucrose solution may help to identify and/or monitor the determinants or regulatory proteins that establish stomatal or nonstomatal cell fate in future studies (Akita et al. 2013).

References

Akita K, Hasezawa S, Higaki T (2013) Breaking of plant stomatal one-cell-spacing rule by sugar solution immersion. *PLOS ONE* 8:e72456

Amor Y, Haigler CH, Johnson S, Wainscott M, Delmer DP (1995) A membrane-associated form of sucrose synthase and its potential role in synthesis of cellulose and callose in plants. *Proc Natl Acad Sci USA* 92:9353–9357

Barratt DH, Barber L, Kruger NJ, Smith AM, Wang TL, Martin C (2001) Multiple, distinct isoforms of sucrose synthase in pea. *Plant Physiol* 127:655–664

Barratt DH, Kölling K, Graf A, Pike M, Calder G, Findlay K, Zeeman SC, Smith AM (2011) Callose synthase GSL7 is necessary for normal phloem transport and inflorescence growth in *Arabidopsis*. *Plant Physiol* 155:328–341

Bergmann DC, Lukowitz W, Somerville CR (2004) Stomatal development and pattern controlled by a MAPKK kinase. *Science* 304:1494–1497

Bieniawska Z, Paul Barratt DH, Garlick AP, Thole V, Kruger NJ, Martin C, Zrenner R, Smith AM (2007) Analysis of the sucrose synthase gene family in *Arabidopsis*. *Plant J* 49:810–828

Chen XY, Liu L, Lee E, Han X, Rim Y, Chu H, Kim SW, Sack F, Kim JY (2009) The *Arabidopsis* callose synthase gene *GSL8* is required for cytokinesis and cell patterning. *Plant Physiol* 150:105–113

Dong J, MacAlister CA, Bergmann DC (2009) BASL controls asymmetric cell

division in *Arabidopsis*. *Cell* 137:1320–1330

Gardner MJ, Baker AJ, Assie JM, Poethig RS, Haseloff JP, Webb AA (2009) GAL4 GFP enhancer trap lines for analysis of stomatal guard cell development and gene expression. *J Exp Bot* 60:213–226

Geisler M, Nadeau J, Sack FD (2000) Oriented asymmetric divisions that generate the stomatal spacing pattern in *Arabidopsis* are disrupted by the too many mouths mutation. *Plant Cell* 12:2075–2086

Guseman JM, Lee JS, Bogenschutz NL, Peterson KM, Virata RE, Xie B, Kanaoka MM, Hong Z, Torii KU (2010) Dysregulation of cell-to-cell connectivity and stomatal patterning by loss-of-function mutation in *Arabidopsis chorus* (*glucan synthase-like 8*). *Development* 137:1731–1741

Hara K, Kajita R, Torii KU, Bergmann DC, Kakimoto T (2007) The secretory peptide gene EPF1 enforces the stomatal one-cell-spacing rule. *Genes Dev* 21:1720–1725

Hara K, Yokoo T, Kajita R, Onishi T, Yahata S, Peterson KM, Torii KU, Kakimoto T (2009) Epidermal cell density is autoregulated via a secretory peptide, EPIDERMAL PATTERNING FACTOR 2 in *Arabidopsis* leaves. *Plant Cell Physiol* 50:1019–1031

Higaki T, Kutsuna N, Hosokawa Y, Akita K, Ebine K, Ueda T, Kondo N, Hasezawa S (2012) Statistical organelle dissection of *Arabidopsis* guard cells using image database LIPS. *Sci Rep* 2:405

Kanaoka MM, Pillitteri LJ, Fujii H, Yoshida Y, Bogenschutz NL, Takabayashi J, Zhu JK, Torii KU (2008) *SCREAM/ICE1* and *SCREAM2* specify three cell-state transitional steps leading to *Arabidopsis* stomatal differentiation. *Plant Cell* 20:1775–1785

Kondo T, Kajita R, Miyazaki A, Hokoyama M, Nakamura-Miura T, Mizuno S,

Masuda Y, Irie K, Tanaka Y, Takada S, Kakimoto T, Sakagami Y (2010) Stomatal density is controlled by a mesophyll-derived signaling molecule. *Plant Cell Physiol* 51:1–8

Kuwabara A, Backhaus A, Malinowski R, Bauch M, Hunt L, Nagata T, Monk N, Sanguinetti G, Fleming A (2011) A shift toward smaller cell size via manipulation of cell cycle gene expression acts to smoothen *Arabidopsis* leaf shape. *Plant Physiol* 156:2196–2206

MacAlister CA, Ohashi-Ito K, Bergmann DC (2007) Transcription-factor control of asymmetric divisions that establish the stomatal lineage. *Nature* 445:537–540

Matsushima R, Kondo M, Nishimura M, Hara-Nishimura I (2003) A novel ER-derived compartment, the ER body, selectively accumulates a beta-glucosidase with an ER-retention signal in *Arabidopsis*. *Plant J* 33:493–502

Pillitteri LJ, Sloan DB, Bogenschutz NL, Torii KU (2007) Termination of asymmetric cell division and differentiation of stomata. *Nature* 445:501–505

Sachs T (1991) Pattern formation in plant tissues. *Cambridge University Press*, Cambridge, UK.

Shpak ED, McAbee JM, Pillitteri LJ, Torii KU (2005) Stomatal patterning and differentiation by synergistic interactions of receptor kinases. *Science* 309:290–293

Sugano SS, Shimada T, Imai Y, Okawa K, Tamai A, Mori M, Hara-Nishimura I (2010) Stomagen positively regulates stomatal density in *Arabidopsis*. *Nature* 463:241–244

Wang H, Ngwenyama N, Liu Y, Walker JC, Zhang S (2007) Stomatal

development and patterning are regulated by environmentally responsive mitogen-activated protein kinases in *Arabidopsis*. *Plant Cell* 19:63–73

Yang M, Sack FD (1995) The *too many mouths* and *four lips* mutations affect stomatal production in *Arabidopsis*. *Plant Cell* 7:2227–2239

Figures

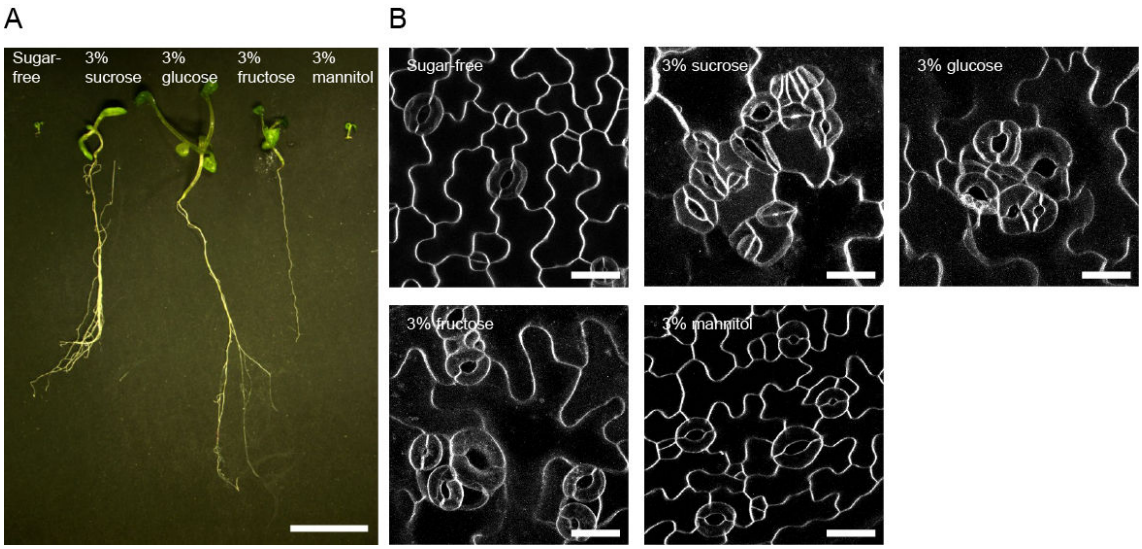

Fig. III-1 Effects of immersion in sugar-free, 3% sucrose, glucose, fructose and mannitol solutions on *Arabidopsis* seedlings and cotyledon guard cell distributions.

(A) Representative 14-day-old seedlings. Scale bar = 1 cm. (B) Fluorescence microscopy images of abaxial cotyledon epidermis stained with FM4-64 dye. Representative images from 10–24 independent seedlings were shown. The maximum intensity projections were constructed with a 0.5 μm step size. Scale bars = 20 μm.

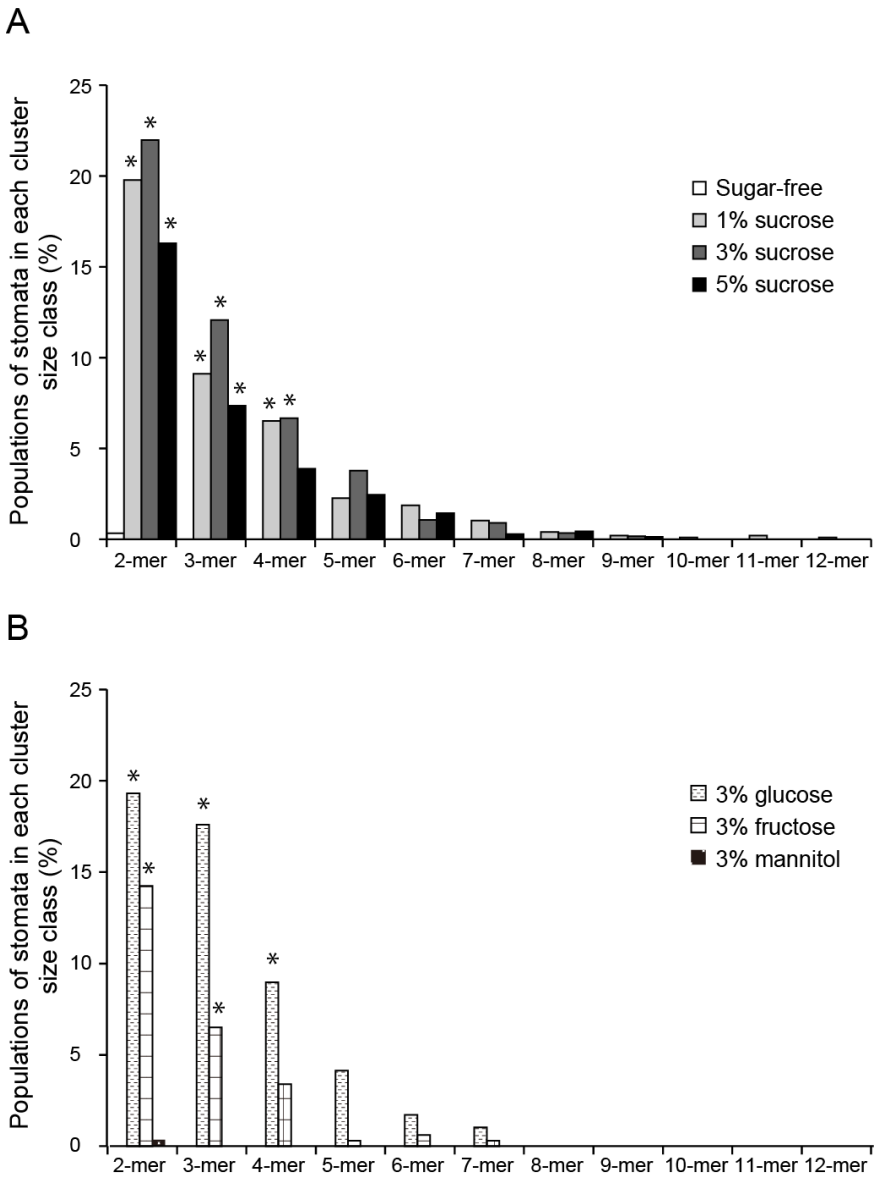

Fig. III-2 Percentage of stomata in each cluster size class.

Abaxial cotyledons from 12- to 15-day-old seedlings grown in sugar-free, 1, 3 or 5% sucrose (A), and 3% glucose, fructose or mannitol (B) solutions were subjected to quantitative analysis. Data are mean values of 20–68 independent observations. Significance with sugar-free conditions was determined using Mann–Whitney's U-test. *p*-value *< 0.0001. Total number of stomata counted: N = 281–1843.

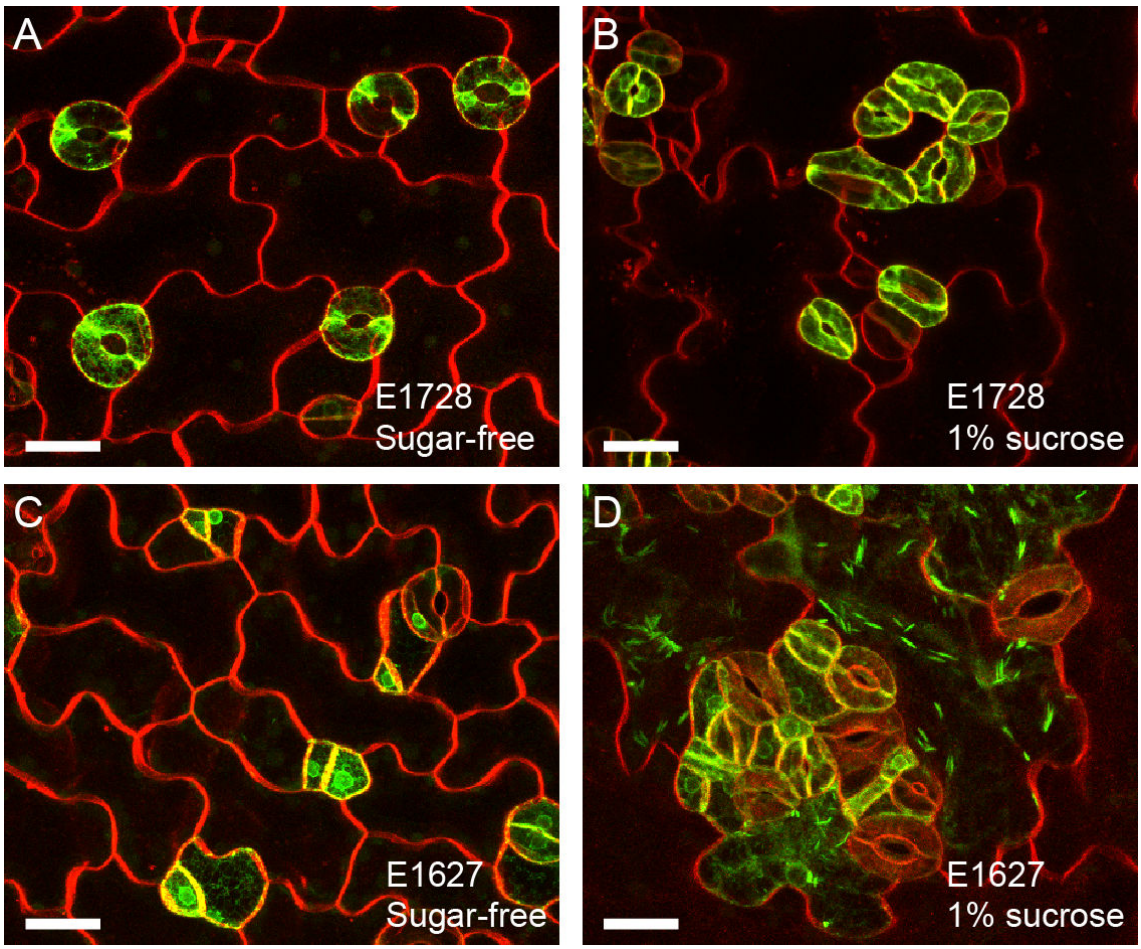

Fig. III-3 Effects of sucrose exposure on stomatal lineage cell markers.

(A and B) Mature guard cell marker E1728-labeled (Gardner et al. 2009) and FM4-64-stained cotyledon epidermis from sugar-free control (A) and 1% sucrose (B) treatments. (C and D) Stomatal cell lineage marker E1627-labeled (Gardner et al. 2009) and FM4-64-stained cotyledon epidermis from sugar-free control (C) and 3% sucrose (D) treatments. Representative images from 10–15 independent seedlings were shown. Note that the jigsaw puzzle-shaped epidermal cells were labeled with E1627 in the sucrose treatment but not in the sugar-free control. Scale bars = 20 μm.

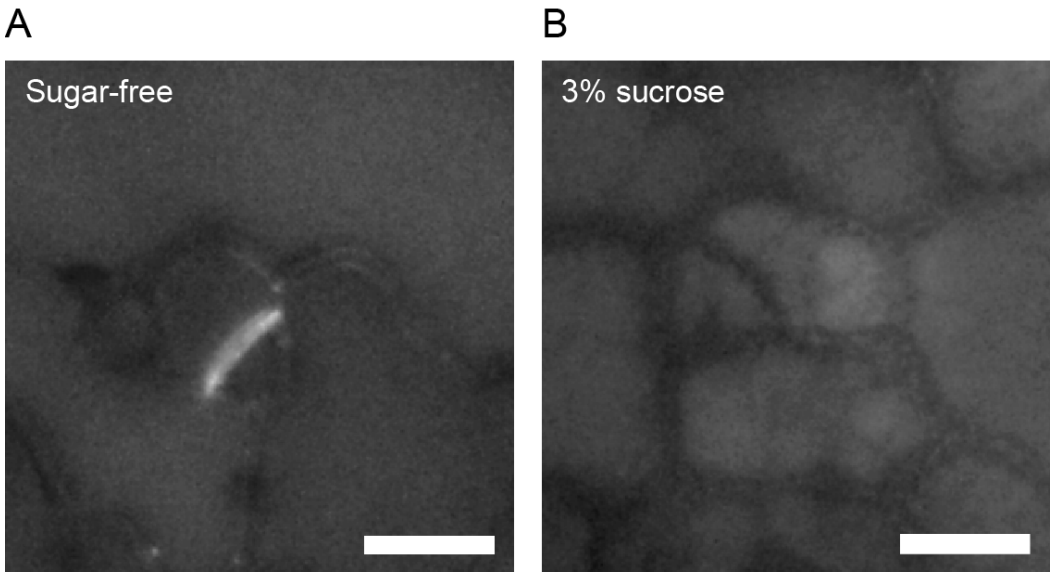

Fig. III-4　Aniline blue staining of cotyledon epidermal cells.

4-day-old cotyledons immersed in sugar-free (A) or 3% sucrose (B) solutions were stained with 0.02% aniline blue for 1 week. Representative images from 24 (sugar-free) and 38 (3% sucrose) independent seedlings were shown. Note that aniline blue fluorescence was clearly detected in new cell walls forming in meristemoids immersed in sucrose-free solutions but not in 3% sucrose solutions. Scale bars = 10 μm.

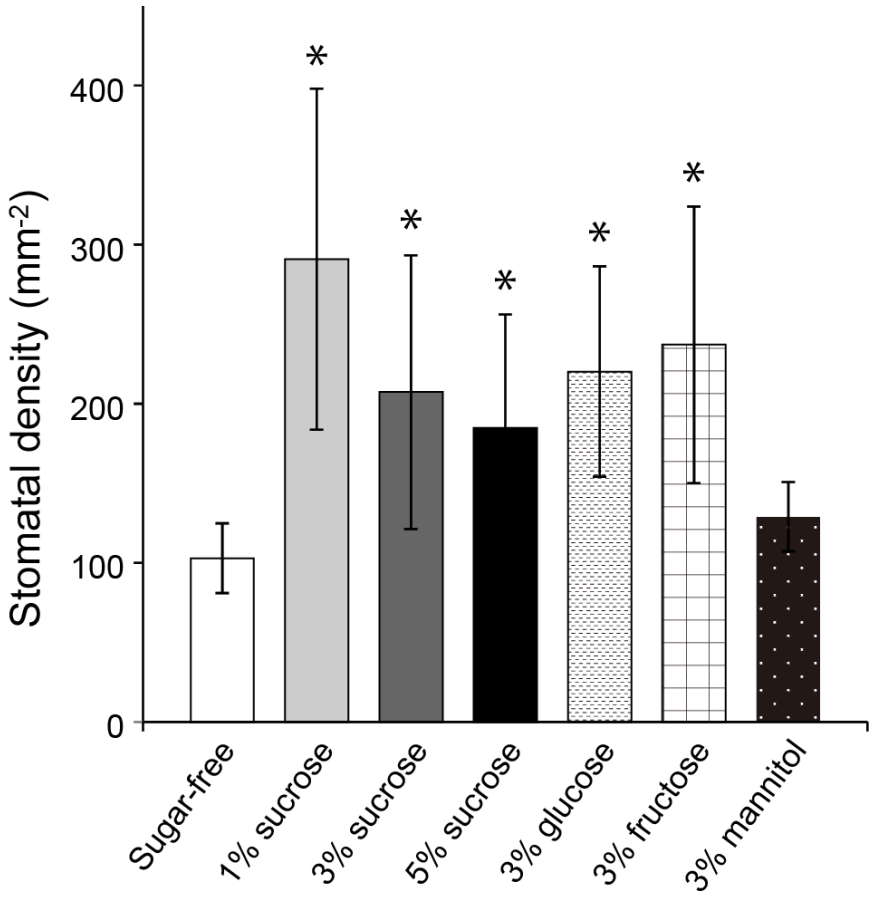

Fig. III-S1 Effects of immersion in sugar-free, 1, 3 or 5% sucrose, 3% glucose, fructose and mannitol solutions on stomatal density.

Data are mean values ± SD of 20–59 independent observations. Significance with sugar-free conditions was determined using Mann–Whitney's U-test. *p*-value *< 0.0001. Total number of stomata counted: N = 281–1843.

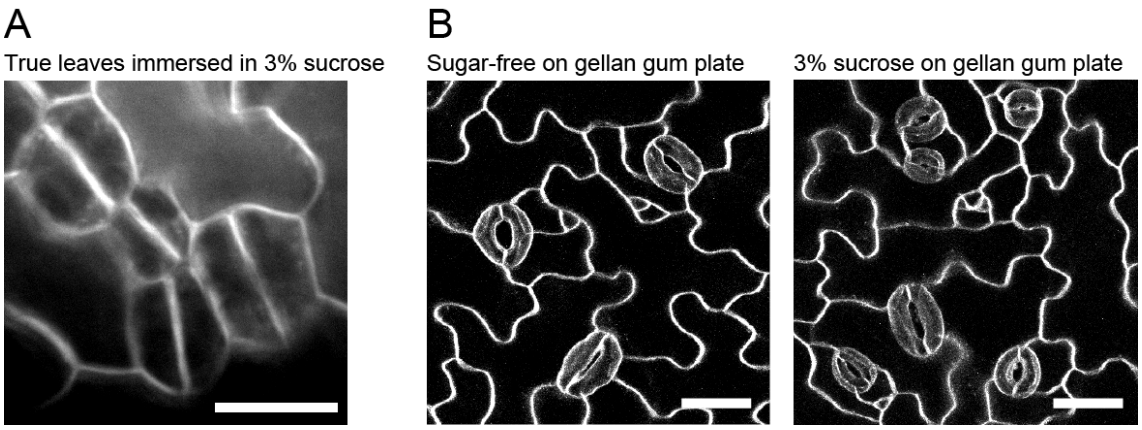

Fig. III-S2　Effects of sugar treatment on stomatal distributions.

(A) Stomatal distribution in the true leaf epidermis of seedlings grown immersed in 3% sucrose solution. Representative images from 10 independent seedlings were shown. (B) Stomatal distribution in the cotyledon epidermis of seedlings grown on a gellan gum plate supplemented with sugar-free (left) or 3% sucrose (right) solution. Representative images from 20 independent seedlings were shown. Scale bars = 20 μm.

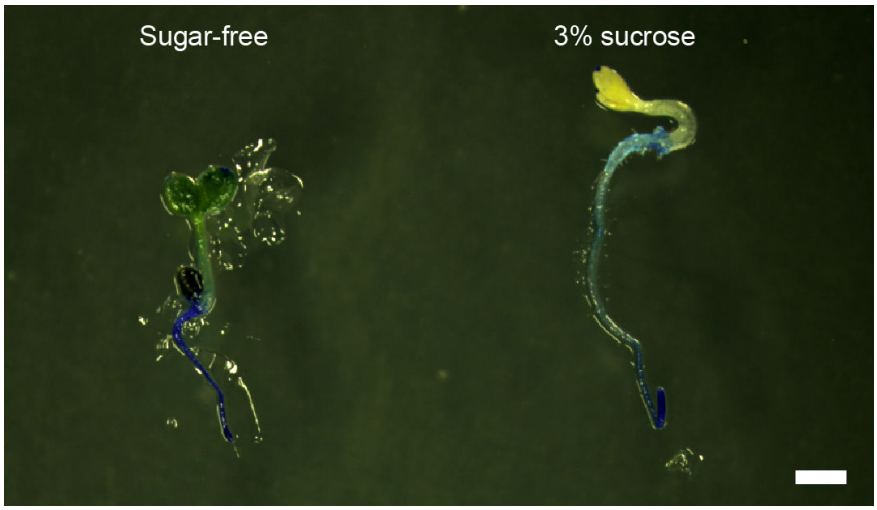

Fig. III-S3　Representative seedlings for aniline blue observations.

4-day-old seedlings with sugar-free (left) or 3% sucrose (right) solution were stained with 0.02% aniline blue for 1 week and then observed. Representative images from 24 (sugar-free) and 38 (3% sucrose) independent seedlings were shown. Scale bar = 1 mm.

General conclusions

To understand the plant leaf epidermis at the cellular level, I researched the cells that constitute the leaf epidermis: pavement cells and guard cells. First, I investigated how pavement cells become shaped like jigsaw puzzle (Conclusive Figure, top). In Chapter I, visualizing exocytosis using the *trans*-Golgi marker ST-mRFP revealed that the secretory pathway targeted to the curved apoplastic region involved in pavement cell morphogenesis. In Chapter II, quantitative evaluations of microtubule orientation showed that microtubules maintained parallel orientations to the pavement cell growth axis. These approaches may help to understand the physiological role of the jigsaw puzzle-shaped in leaf pavement cells in the future.

Second, I investigated the effect of external conditions on the stomatal spacing distribution (Conclusive Figure, bottom). In Chapter III, I showed that sugar solution immersion changed the cell fate through compromised cell walls and induced clustered stomata in the leaf epidermis. This result demonstrated that cell walls affect not only cell morphology but also cell fate.

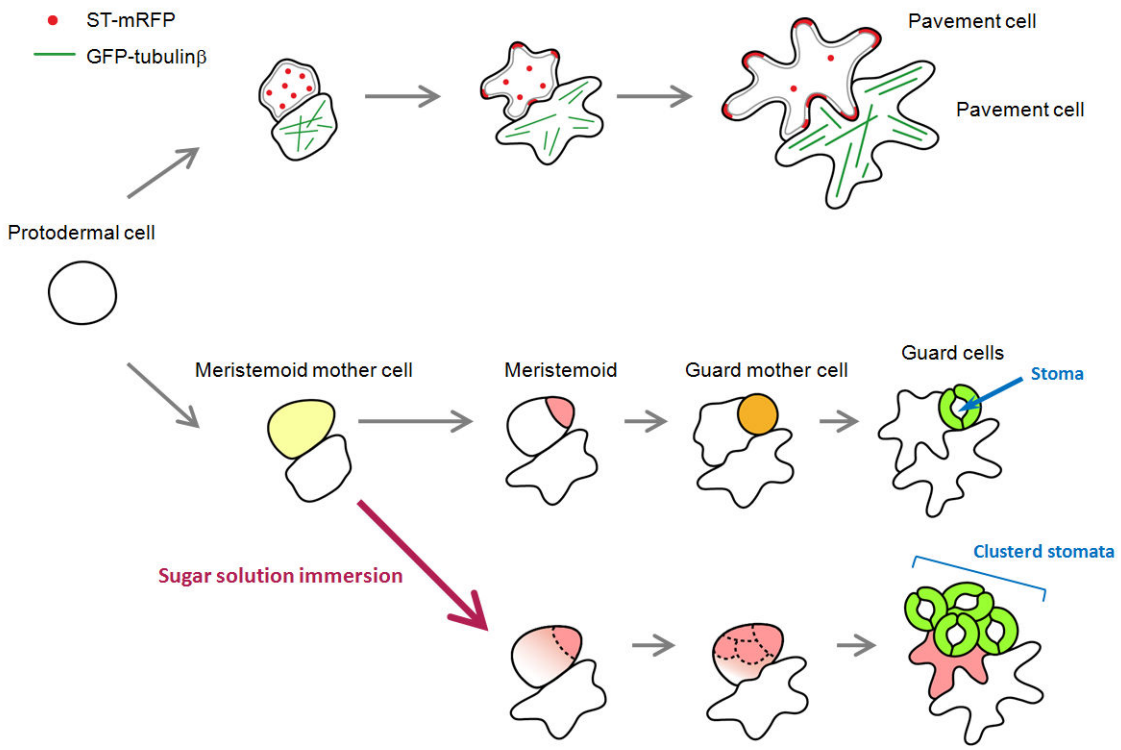

Conclusive Figure

Overview of this study's hypothesis. Undifferentiated protodermal cells differentiate into pavement cells or into guard cells through stomatal lineage cells. During differentiation into pavement cells, the secretory pathway labeled by ST-mRFP targeted curved apoplastic regions and microtubules visualized with GFP-tubulinβ maintained parallel orientations to the growth axis. When *Arabidopsis* seeds were immersed into sugar solution, unidentified cell-fate determinants (pink) leaked through compromised cell walls, and, as a result, clustered stomata appeared.